COHERENT COOLANT DELIVERY IN GRINDING

A STUDY OF COHERENT JETS AND THEIR ABILITY TO DELIVER GRINDING FLUID

BY

MAXWELL LIGHTSTONE, B.Eng.

A THESIS

SUBMITTED TO THE DEPARTMENT OF MECHANICAL ENGINEERING

AND THE SCHOOL OF GRADUATE STUDIES

OF MCMASTER UNIVERSITY

IN PARTIAL FULFILMENT OF THE REQUIREMENTS

FOR THE DEGREE OF

Master of Applied Science

Master of Applied Science (2021) McMaster University

(mechanical engineering) Hamilton, Ontario, Canada

TITLE:	A Study of Coherent Jets and their Ability to Deliver Grinding Fluid
AUTHOR:	Maxwell Lightstone B.Eng. (Mechanical Engineering), McMaster University, Hamilton, Canada
SUPERVISOR:	Dr. Philip Koshy, PhD PEng Dr. Stephen Tullis, PhD PEng
NUMBER OF PAGES:	xvi, 113

Abstract

Coolant application is critically important in grinding, preventing workpiece damage and increasing the quality of manufactured components. However, delivery of grinding fluids is difficult to achieve, due to issues unique to grinding processes such as the air layer that surrounds the wheel. Coherent jets, which maintain their shape over a significant distance, are one of the most effective methods of coolant delivery and a significant amount of research has been devoted to developing them. Results of this work, which has largely focused on contoured nozzles, have been modest.

Inspired by laminar fountains and wind tunnel design, the present work focuses on the development of a coherent, laminar jet. The developed jet possesses extreme coherence, and appears to resemble a glass rod with its stability and clarity. Investigations were carried out, comparing the coherence and cooling ability of the developed system to that of a commercially available coherent nozzle. Models for the structure of the air layer and to predict the conditions necessary for a jet to penetrate the air layer were also developed. The developed jet outperformed the commercial system both in terms of coherence and manufacturing productivity. The model was validated with experimental values, and appears to provide excellent agreement to those results.

This work details the background, design, and experimentation involved in creating these innovative systems.

To my parents

who taught me to explore the world

Acknowledgements

This degree has been the hardest thing that I have ever done, but also the most rewarding. I would like to acknowledge and thank everyone who has helped me get to where I am today, and supported me along the process.

I would like to thank my advisors, Dr Koshy and Dr Tullis, for their guidance, ingenuity, experience, and advice. Their support made this a reality, in every way.

I would like to thank Natalie Martin and Lilia Fuller-Thomson, my colleagues and friends who started this journey with me in our undergraduate capstone project. I think that all three of us can agree that it was a good first choice.

I would like to acknowledge and express my gratitude for all the staff in the Department of Mechanical Engineering, in the office, the machine shop, and the MMRI. From guidance on design, to assistance with maintenance, to pushing schedules in the middle of a pandemic, their support was invaluable.

I would like to pay special attention to my friends and colleagues in graduate school, from Advanced Fluid Mechanics classes to seminar, and from the Engineering Graduate Society to teaching duties. They are too numerous to name here, but I couldn't have done it without them.

Finally, to my family. You are always there when I need you, from 2 in the afternoon to 2 in the morning. You are always there with smiles and commiseration, support and celebration, and I appreciate you above all else. And to my younger brother Adi, I know that whatever happens, I'll always have a friend.

Contents

List of Figures

List of Tables

List of Symbols and Abbreviations

a_e	Depth of cut	µm
A_j	Area of the jet	m^2
A_n	Area of the nozzle	m^2
b	Wheel width	m
C_C	Contraction coefficient, calculated with eqn. 2.14	
d_g	Mean grain diameter, calculated with eqn. 2.4	mm
d_j	Jet diameter	m
f	Wheel pore filling factor	
F_T	Tangential force applied by the wheel	N
g_s	Abrasive grit specification	
h_{air}	Average height of the air layer	m
$h_{eq,geo}$	Equivalent surface film thickness, calculated with eqn. 2.2	m
h_{free}	Equivalent surface film thickness supported by air pressure, calculated with inequality 2.5	m

K	Pressure drop coefficient The ratio of the drop in static pressure to the dynamic pressure of a flow. Calculated with equation 2.21.	
L_{dev}	Development length The distance required for an internal flow to become fully developed. Calculated with eqn. 2.18	m
M	Per unit width momentum flux, frequently shorthanded to just *momentum*	kg/s^2
M'_{j}	Effective jet momentum, accounting for the impact angle. Calculated with eqn. 2.13	kg/s^2
p	Pressure	Pa
P_{m}	Machining Power	W
r	Wheel radius	m
R_{t}	Surface roughness, calculated with eqn. 2.10	µm
Re_x	The Reynolds number, calculated with the characteristic length x	
t	Distance away from the wheel surface	mm
T	Temperature	°C
u	Air layer velocity	m/s
$u(t)$	Air layer velocity as a function of distance away from the wheel surface	m/s
$u'(t)$	Nondimentional air layer velocity	

v_j	Jet speed	m/s
v_s	Wheel surface speed	m/s
$\dot{V}$	Volumetric flow rate	m^3/s
$\dot{V}_{c,f}$	Free carrying capacity The maximum amount of grinding fluid that can be supported on the wheel surface.	m^3/s
$\dot{V}_{c,g}$	Geometric carrying capacity The maximum amount of grinding fluid that can be transported into the contact patch in pores on the wheel surface.	m^3/s
α_n	Nozzle orientation or jet orientation relative to the wheel normal vector	$^\circ$
α_t	Nozzle orientation or jet orientation relative to the wheel tangent	$^\circ$
ε	Kinetic Energy coefficient, a value that can be used to describe the velocity profile of a flowing fluid. It is calculated from eqn. 2.19	
Θ	Momentum thickness	m
Ξ	Coherency, measure of how much a jet has spread over a distance. Calculated with equation 3.3	
ρ	Density	kg/m^3
φ	Wheel porosity, calculated with eqn. 2.3	%

Chapter 1

Introduction

Grinding is an abrasive manufacturing process that has been used since the advent of anatomically modern humans hundreds of thousands of years ago [1]. It has been, and continues to be, used in a variety of applications including food production and metal cutting (hereafter referred to as manufacturing) [1, 2]. Modern grinding in manufacturing applications utilizes hard abrasive grains held in a matrix to remove metal with small and precise passes. Grinding is used over other manufacturing processes such as milling or turning because of its ability to provide high dimensional accuracy, excellent surface finishes, relatively high material removal rates on difficult to machine materials, and the ability to machine hard or brittle materials [2]. In any manufacturing process, the majority of consumed energy becomes waste heat [3]; unlike other processes where much of this heat can be removed by the discarded chips [3], in grinding the majority of the heat flows into the workpiece [4]. Grinding is also unique for the amount of energy consumed per unit of material removed, which can be orders of magnitude higher than in turning or milling [5]. If inadequately managed, the thermal energy can result in oxidation, poor surface finishes, subsurface

phase transformations, and potentially surface cracking [4,6]. Grinding fluids are the primary method used to reduce thermal effects – and others, including mechanical and chemical effects – on the workpiece [7].

1.1 Importance of Effective Cooling in Grinding

In their 2020 keynote paper to the International Academy for Production Engineering (CIRP), Heinzel et al list the following benefits of effective coolant delivery [8]:

- Cooling the workpiece, which lessens the thermal impact
- Cooling the wheel itself
- Lubricating the wheel-workpiece interface, which reduces friction, energy consumption, and heat generation
- Cleaning the wheel, and removing swarf (chips and wheel particles that can clog the wheel)
- Improved dimensional control and accuracy over the final manufactured part
- Increased lifespan of the grinding wheel

All of these concerns, in the end, have an impact on productivity. A manufacturing process will be carried out faster due to deeper cuts, lower maintenance time, and better accuracy, or less expensively due to lower energy requirements and longer tool life spans. Increased productivity and decreased operating costs can only have positive impacts on a business's bottom line. Setting wheel cleaning aside, grinding fluids

provide the key mechanisms that benefit the grinding process: cooling and lubrication [9]. Inadequate or ineffective grinding fluid application can cause catastrophic outcomes, including warping and cracking. Moreover, in certain cases the electrical power required to drive the coolant pump can be almost two-thirds of the total energy consumption of a grinding process [5], while the effective flow rate (the proportion of applied fluid that enters the grinding contact patch) may be as low as 4% [10]. Addressing issues in coolant delivery must be a priority of researchers and operators.

1.2 Issues Affecting Effective Coolant Application

Issues with coolant application may be stated succinctly, if simplistically, as it is difficult to saturate the wheel-workpiece interface with coolant. There are three primary mechanisms that are responsible for this difficulty: the air that coats the wheel's surface and that is pumped radially though the wheel side faces (1), the centrifugal force that acts to fling the coolant off of the wheel (2), and the geometrical difficulties of getting the fluid between the wheel and the workpiece (3) [11–13]. These three difficulties stem from the two methods that can be used to deliver coolant: by directly filling the converging wedge or by wetting the wheel surface and depending on the wheel to rotate the fluid film into the contact patch [14]. A low velocity jet of fluid directed towards the wheel periphery will be deflected by the layer of air without wetting the surface. If the jet has a high enough velocity to break through the air layer, much if not all of the fluid will be cast off by centrifugal force, never reaching the grinding zone. To avoid this issue, the coolant may instead be directed straight towards the converging wedge. Here, however, there is the issue of aiming amid the grinding geometry, as well as other effects of the air layer. Grinding can often involve

complicated or awkward geometries that make it difficult to mount a nozzle close to the converging wedge, which is necessary when using common nozzles that tend to spray [13]. Furthermore, when the previously discussed air layer reaches the converging wedge, it is compressed and reversed back away from the grinding wheel. This area of reversing flow pushes away any coolant directed towards it [15,16]. Unless the air layer is managed, any grinding coolant that reaches the grinding zone will have been mixed into a two phase air-coolant mixture, and will be ineffective at lubrication or cooling.

1.3 The State of the Art

Considerable work has been done over the last fifty years to address these issues and to optimize coolant delivery; that is to say maximize the delivered coolant while minimizing waste. Much work has focused on controlling the air layer, including scraping it away from the surface of the wheel or covering the flat faces of porous wheels to prevent air from being drawn in and expelled at the surface [14, 17, 18]. Other works have focused on ways to penetrate the air layer, including what jet speed and nozzle orientations allow for the best delivery of coolant [15, 18]. Mechanisms of coolant delivery have been considered in depth. Some of these are refinements of previous methods, such as nozzles designed to generate coherent jets, which hold their shape and resist diverging and spraying [19,20], or the shoe nozzle, which is positioned adjacent to the wheel surface near the converging wedge, and supplies coolant at low pressures while its own structure removes the air. Other, more innovative options, including through-wheel coolant delivery [8] and "painting" lubricating oil onto the wheel surface with a brush [21] have been developed.

1.4 Contributions of the Current Work

The present work focuses on the issue of precise delivery of coolant to the grinding zone using coherent jets. Mentioned above, a coherent jet is one that retains its shape as it traverses the distance from the nozzle to its target, without slowing or dispersing. A coherent jet is beneficial to coolant delivery because it is more effective at penetrating the air layer or the reversing air flow, and because it can be aimed accurately from greater distances than a conventional diffuse jet. Inspired by ornamental water features (example in figure 1.1), a highly effective flow conditioner and nozzle were developed. The coolant delivery system created herein utilizes fluid mechanics principles to ensure a laminar flow free of eddies, velocity variations, or perturbations upstream of the nozzle. This research investigated the resultant jet considering both breakup and coolant delivery compared to the state of the art in commercially

Figure 1.1: Laminar jet fountain at the Detroit Metro airport (Courtesy of Wet Design)

available nozzles. These observations were validated and a grinding burn test demonstrating the real-world effectiveness of the delivered coolant was performed, showing the achievable productivity before workpiece damage.

Chapter 2

Literature Review

This review is divided into two primary sections: *Coolant Mechanics* and *Coolant Application Methods*. The first section, coolant mechanics, focuses on the grinding fluid as it interacts with grinding processes themselves. This includes heat transfer from the wheel and workpiece to the fluid, the mechanisms by which the fluid is carried through the grinding zone, and measurements of how effective a particular coolant delivery technique is. Coolant application methods, the second section, is concerned with the issues and techniques involved with introducing fluid to the wheel and the grinding contact patch. Topics covered include different methods of coolant introduction, the issue of the air layer, nozzle design, and coherent jets.

This literature review provides an in-depth investigation into the state of the art, as well as a foundation for the reader to fully understand the experimental direction.

2.1 Coolant Mechanics

Coolants are critical to the grinding process, but as discussed below, coolant application is very inefficient [10]. While grinding may account for up to 80% of a product's cost [22], cooling alone can make up to 17% of the total manufacturing cost [23]. It has also been noted that coolant supply can account for more than 25% of total energy costs [24]. Small increases in the effectiveness of cutting fluid application can have dramatic benefits to the operator.

2.1.1 Heat Transfer

A significant amount of heat is generated in the grinding zone, due to chip formation, rubbing between the grains and the workpiece, and ploughing [6]. The latter two mechanisms are considered 'unproductive' as they remove no material [25], and Malkin noted that the energy consumed by them is converted to heat, along with the productive cutting energy [4]. The generated heat is conducted away from the grinding zone into the wheel grains, removed chips, and the applied grinding fluid [26], but the majority (above 70% in a generic grinding operation) flows into the bulk of the workpiece [27, 28]. This may be contrasted to a cutting operation, where 90% of the heat can be carried by the chips [27]. Malkin noted that the energy used was considerably higher than the energy required to entirely melt the chips, which ranges from below 5 to above 15 J/mm^3 for various materials [4] and is around 10.5 J/mm^3 for steel [25], which would make it impossible for the chips to have a significant heat sink impact. Table 2.1 shows some sample energy partitions that have been reported for cutting and grinding processes.

If the heat is not managed properly, it can lead to thermal damage such as tensile

Table 2.1: A selection of energy partitions from literature

Percentage of heat flow into...	Cutting operation [27]	Generic grinding process [29]	Grinding with CBN wheel [29]	Fine grinding process [27]
The tool	5%	8%	30%	20%
The workpiece	5%	72%	45%	80%
The chips	90%	10%	20%	0%
The coolant	–	10%	5%	–

residual stresses, discolouration, softening, rehardening, and cracks [25]. Coolant is typically used for this purpose, for both removing the heat and lubricating the grinding zone to reduce the amount of heat that is produced. The coolant removes heat through different processes depending on the temperature of the workpiece. If the wheel-workpiece interface is at a low enough temperature, the heat transfer between it and the grinding fluid will be through simple convection. As the surface temperature increases, the heat transfer mechanism changes to nucleate boiling. Nucleate boiling is marked by bubble generation, forced convection, and higher heat transfer rates. Still higher temperatures will lead to film boiling, where the liquid immediately turns to vapour upon contact with the hot surface, and forms a thermal barrier between the pool of liquid and the workpiece [26]. Since the liquid is prevented from contacting the work surface, and water vapour has a considerably lower density and thermal conductivity compared to liquid water, the heat flux plummets and the temperature of the workpiece increases dramatically [30]. Shown as the point of Critical Heat Flux (CHF) in figure 2.1, this transition occurs around 130° C for water [13].

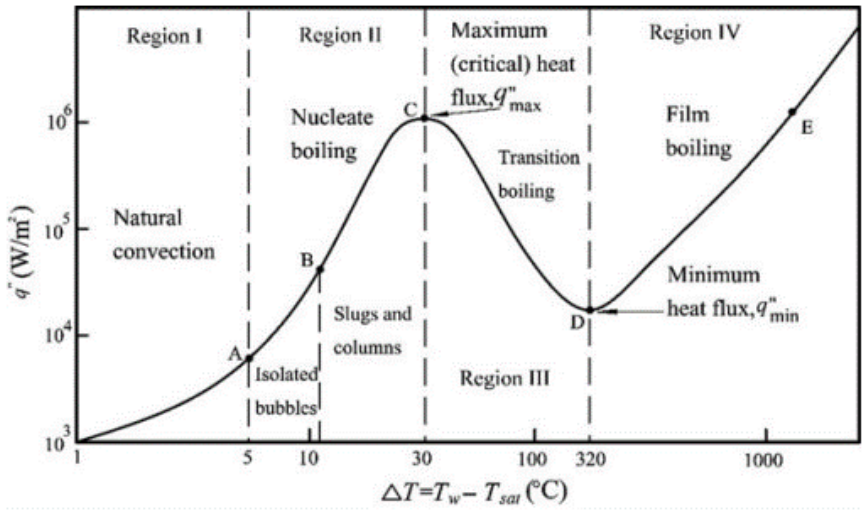

Figure 2.1: Boiling curve for water [31]

2.1.2 Mechanisms of Coolant Transportation

In order to be effective, coolant needs to be transported from the nozzle to the contact patch between the wheel and the workpiece. Akiyama [14] lists two main processes by which this can happen: the converging zone can be flooded with fluid which is then dragged by the wheel, or the fluid can be carried on the surface of the wheel as a thin film.

Both methods are limited by the physical amount of fluid that the wheel can carry and deliver, which can be referred to as the geometric carrying capacity. The fluid is carried between grains and inside pores on the wheel surface and the degree to which the pores are filled can vary based on the wheel's density and porosity, with the pores on low density wheels filling up more than those on high density wheels [32, 33]. This can be ascribed to the difficulty involved in displacing the air inside those pores. The geometric carrying capacity can be predicted with equation 2.1 [34], where f is the aforementioned filling factor, φ is the wheel porosity, d_g is the mean grain diameter, b

is the wheel width, and v_s is the wheel speed. Morgan [34] assumes a standard filling factor of 50%.

$$\dot{V}_{c,g} = f \cdot \varphi \cdot d_g \cdot b \cdot v_s \tag{2.1}$$

This carrying capacity can be divided by the wheel width and wheel speed to provide an equivalent surface film thickness.

$$h_{\text{geo,eq}} = f \cdot \varphi \cdot d_g \tag{2.2}$$

Malkin and Guo [35] offer a prediction for the porosity based on the wheel's grade letter and structure number, and of the mean grain diameter. If $n = \{\ldots, -1, 0, 1, 2, 3, \ldots\}$ for the grade letters $\{\ldots$,C,D,E,F,G,$\ldots\}$, and s is the structure number, the percent porosity can be estimated with equation 2.3.

$$\%\varphi = 45 + \frac{s - 2n}{1.5} \tag{2.3}$$

The mean grain diameter can be estimated with equation 2.4, where the value is in mm and g_s is the abrasive grit specification [32, 35].

$$d_g = \frac{15.2}{g_s} \text{ [mm]} \tag{2.4}$$

This prediction of the geometric carrying capacity provides an upper limit to the amount of coolant that can be effectively delivered, as any additional supply would be wasted. This has been shown by Morgan et al [34] who showed that the useful flow rate increased linearly with wheel speed at a constant jet flow rate, in line with predictions.

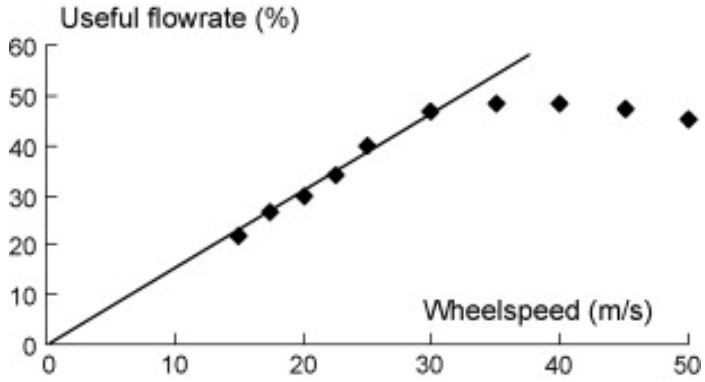

Figure 2.2: Useful flow rate as a function of wheel speed [34]

In the second method there is an additional value to be considered, which is the volume of fluid that can be supported on the free surface of the wheel. Since the wheel is revolving at a high speed, a considerable centrifugal force is applied to the fluid film. Several mechanisms have been posited to act in opposition to the centrifugal force and hold the film in place, including surface tension [36], van der Waals forces [14], and an air pressure differential that is similar to the Coanda effect [21,37]. The adherence force will balance the centrifugal force at a certain film thickness. This film thickness, multiplied by the wheel width and velocity, provides a free carrying capacity.

Gvinishvili [37] uses the difference between the atmospheric air pressure and the static air pressure adjacent to the wheel surface to balance the centrifugal force, and proposes the following inequality:

$$\frac{\rho \cdot h_{\text{free}} \cdot b \cdot v_s^2}{r} \leq (p_a - p_s) \cdot b \tag{2.5}$$

In this inequality, ρ is the fluid density, h_{free} is the free film thickness, r is the wheel radius, and p_a and p_s are the atmospheric and wheel-adjacent pressures respectively.

The free carrying capacity could then be calculated with equation 2.6:

$$\dot{V}_{c,f} = h_{\text{free}} \cdot b \cdot v_s \tag{2.6}$$

If the free carrying capacity is larger than the geometric carrying capacity, issues such as the reversing air flow at the converging wedge can be completely avoided by transporting the fluid on the wheel surface, without detriment.

2.1.3 Measures of Cooling Effectiveness

The application of coolant in a grinding process is only useful when it is effective at removing heat. There have been several ways proposed and used by researchers to determine how effective a coolant delivery method has been, including measuring the effective flow rate, determining the onset of grinding burn, and others such as surface quality of the finished part and the power consumption. Effective flow rate is a direct measure of the amount of coolant delivered by the nozzle that makes its way through the grinding zone. Grinding burn as a method for examining effectiveness is more recent, and is based on the idea that if a method is more effective at delivering coolant, it will delay the onset of film boiling and the subsequent burn of the workpiece.

Beyond these two techniques, many other methods have been used to determine how effective a system is at cooling a grinding process.

Sakamoto et al [38] and Majumdar et al [39] used the roughness of the ground surface as an indication of the cooling effectiveness. Since the ultimate objective of a grinding process is to obtain good dimensional accuracy and surface finish, resultant roughness is a measure of the overall grinding process quality.

Measurements of grinding responses have also been used to determine coolant

delivery effectiveness. Given that the grinding fluid has the dual role of lubricating and cooling, a change in spindle power or applied forces would indicate the relative impact of the fluid. Several groups [32, 39–41] measured the tangential and normal forces on the workpiece from the grinding wheel, from which the power consumption of the grinding process could be calculated using equation 2.7, where F_T is the tangential force that the wheel imparts on the workpiece, and v_s is the wheel speed.

$$P_m = F_T \cdot v_s \tag{2.7}$$

Power and forces can be used to contrast coolant delivery effectiveness between trials in a consistent setup, or can be normalized against the material removal rate to find the specific grinding energy, as was done by Majumdar [39]. In a similar approach, Kirsch measured the hydrodynamic pressure generated beneath the wheel, which provides an indication of how much fluid is transported between the wheel and the workpiece [40].

Heinzel et al [42], Jackson [32], and Liu et al [43] used direct measurements of the temperature under the grinding wheel to compare coolant effectiveness between cases. Jackson ran a wheel over a workpiece embedded with a wire thermocouple. Heinzel combined the thermocouple approach with optical sensing using a fiber optic in the wheel to confirm the collected data. Uniquely, their work had a wheel plunge into a workpiece that had a heater and a thermocouple embedded beneath the surface. The electric heater heats the workpiece at a constant rate (constant supplied power), and the wheel is rotated above it. This allowed the investigation of the cooling effect of the working fluid as it interacted with the grinding wheel, while significantly reducing experimental uncertainty [42]. Liu took thermal images of the workpiece to observe

the impact of the coolant on the process, noting that fiber optics were unusable above 300 degrees [43].

Effective Flow Rate

Effective flow rate is the measure of the portion of applied grinding fluid that is carried by the grinding wheel through the contact patch. One of the first attempts at measuring the effective flow rate was done by Akiyama et al in 1984 [14]. A grinding wheel was passed over an electrode, and the electrical resistance between the electrode terminals was measured. After accounting for thermal effects, the researchers were able to determine the mean fluid film thickness, which could be multiplied by the wheel width and surface speed to find the effective flow rate. In 1992, Engineer et al [10] developed a system to directly measure the amount of fluid that was carried by the wheel and ejected after the contact patch, pictured in figure 2.3. In their design, the grinding wheel was passed over a workpiece attached to a collection tray. Side scrapers, moving with the wheel, were used to ensure that only fluid which passed beneath the wheel was collected. Engineer's method formed the basis for the majority of subsequent designs, including those developed by Jackson [32], Li et al. [44], and Madanchi et al [24].

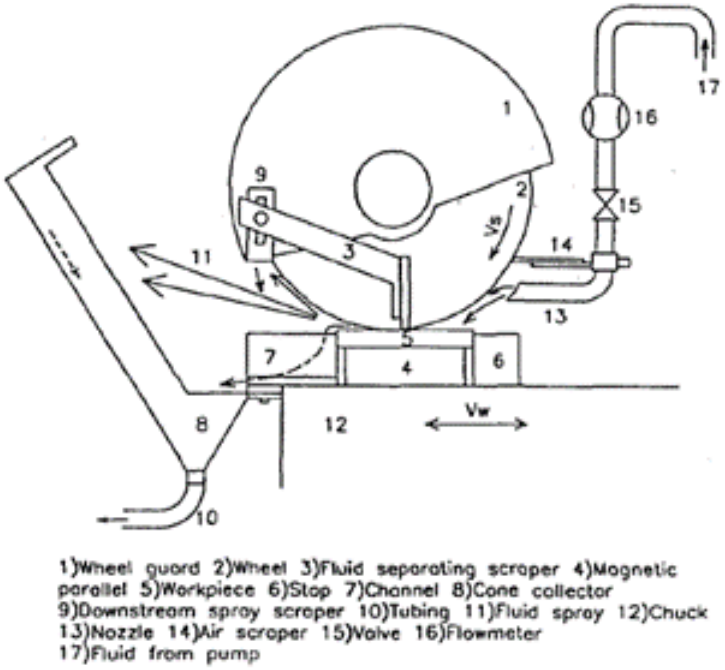

Figure 2.3: Effective flow collection system [10]

Grinding Burn

Grinding burn, also known as burnout, is thermal damage to a workpiece due to ineffective control of grinding temperature. It occurs upon the transition from nucleate boiling to film boiling, when the applied coolant cannot manage the generated heat. According to Badger and Torrance [6] there are four degrees of grinding burn: Oxidation burn, thermal softening, residual tensile stresses, and rehardening burn. Oxidation burn shows up upon visual inspection as a discolouration on the surface of the workpiece – an example of which can be seen in figure 2.4 - but visual cues are neither the only nor necessarily the most effective method of determining the onset of grinding burn. Others include both instantaneous and post grind pass tests, such as power measurements and residual stress analyses.

In a power based burn test, the spindle power is recorded as grinding passes are

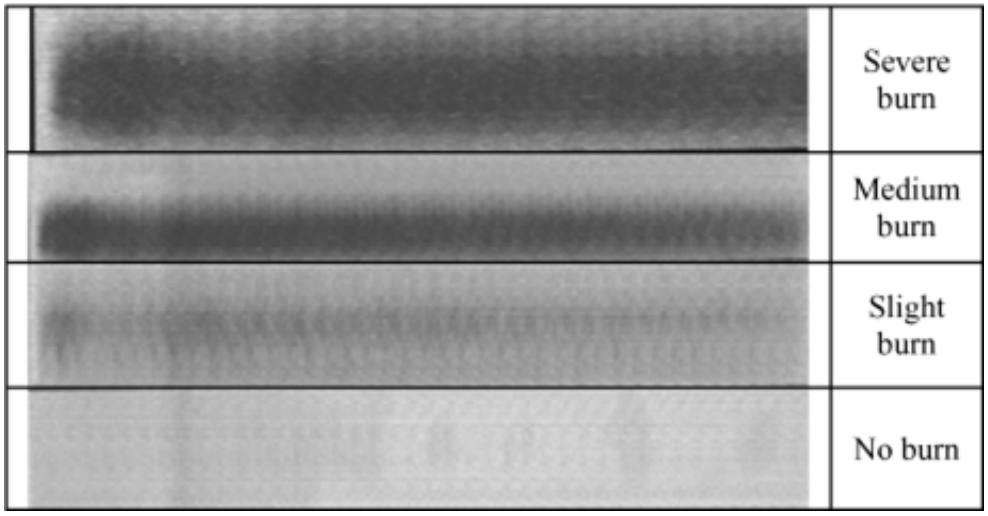

Figure 2.4: Examples of varying degrees of surface grinding burn [30]

made with increasing cutting depths, as spindle power increases predictably with the depth of cut and material removal rate until burn occurs. When this happens, there is an observable "surge" in the wheel's power consumption which is attributed to the fact that the wheel is essentially grinding dry without lubrication [13]. Other researchers noted that burn is accompanied by the wheel itself becoming rougher and adhering to the workpiece, which increases the grinding force and spindle power, as shown in equation 2.7 [4]. To avoid the trouble of taking repeated passes, several researchers performed a single grinding pass on a sloped workpiece, and observed the power consumption throughout, stopping the test when the surge occurred. Webster used a workpiece sloped at 1.5° [13], and Steffen used an incline of 2° [45]. Results from Steffen's experiments showing the surge can be seen in figure 2.5.

Other tests include NITAL etching (an optical metallographic investigation), Barkhausen noise analysis, residual stress tests, and hardness change investigations [13, 45]. Webster used each of these techniques, and found them to provide critical material removal

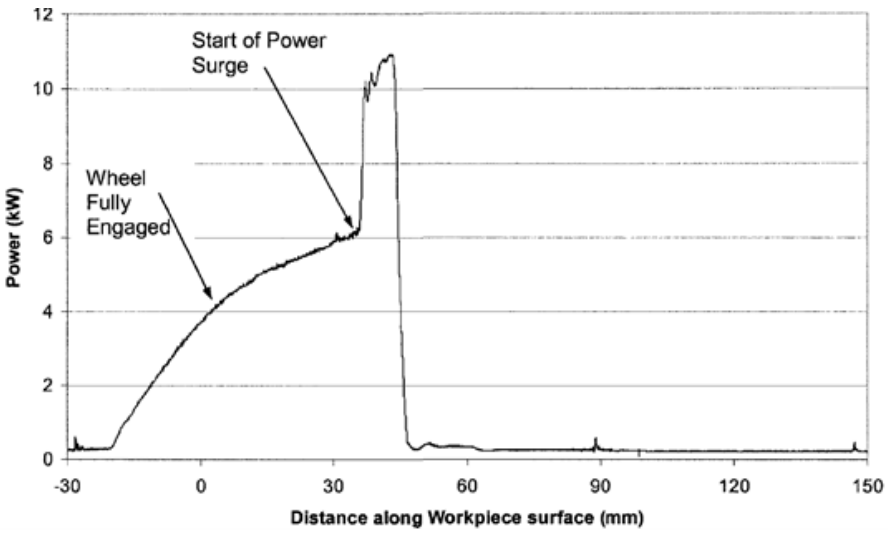

Figure 2.5: Power surge accompanying burn [45]

rates within 1 mm^3/s of one another, and found that a test of residual stress increases was able to detect the thermal impact the earliest.

2.2 Coolant Application Methods

Coolant is critical in grinding processes, and ineffective coolant application will have a significant impact on manufacturing outcomes, affecting productivity, dimensional tolerances, and surface quality. The primary objective is getting grinding fluids into the space between the wheel and the workpiece, but the air layer and other complexities of the grinding process make that difficult.

Penetrating the air layer has been the focus of a plurality of this review. The structure and strength of the air layer was considered, as were the two competing ideas of how best to traverse it. The best method for coolant delivery in high-speed grinding, based on flexibility and the depth of research conducted, is though the use of free, coherent jets. These jets maintain their shape and their momentum and can be accurately aimed as well as effectively penetrate the air layer or the reversing air flow. Different methods of generating a coherent jet were reported, as was the principle that the methods can be combined with synergistic effects.

Currently used techniques to create a high-speed coherent jet leave much to be desired. The state of the art includes jets that quickly diverge, or which have significant surface waves and air entrainment. There is much room for improvement, which will be the focus of this work.

2.2.1 Application Types

Several methods of delivering coolant to the grinding zone have been developed and are used in research and industry, ranging from flooding the workpiece to direct application of the liquid on the wheel surface. The application method has a significant impact on the issues faced, but each method adds complexities of their own.

Flood Cooling

Flood cooling is a simple coolant delivery process that delivers large amounts of fluid to the grinding zone at low velocities and pressures [7]. In flood cooling, nozzle flow rates are typically on the order of 10-100 liters per minute [24], but the effective flow may be as low as 4% of that value [10]. This is due to the ineffectiveness of the low pressure coolant at penetrating the air layer [25], which can be seen in figure 2.6. Marinescu noted that flood cooling is unlikely to be effective for high wheel speeds, and that imprecise nozzle positioning leads to poor grinding performance [25].

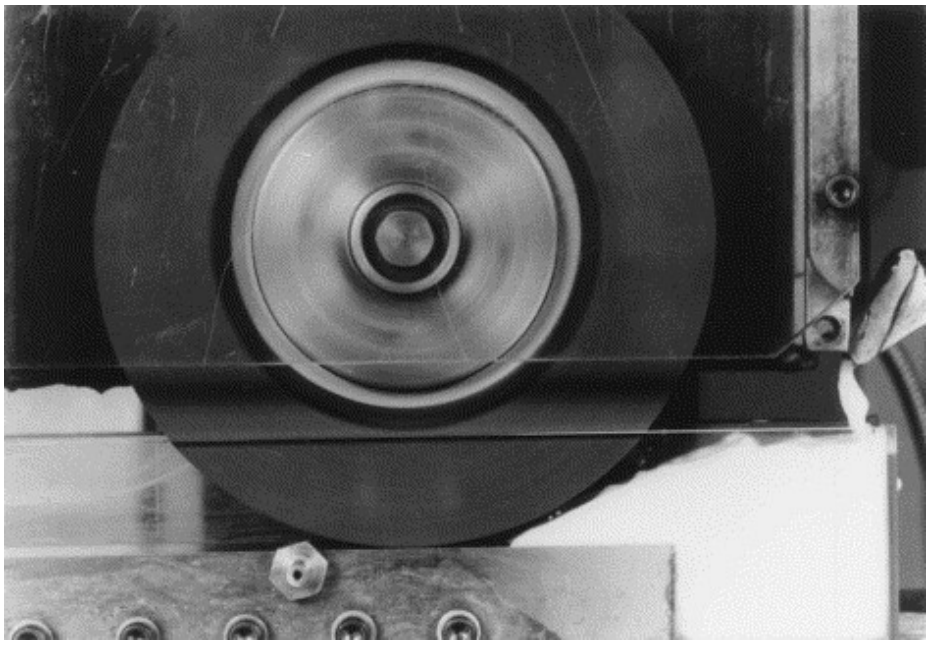

Figure 2.6: Air layer preventing fluid delivery in low pressure flood cooling [15]

Jets and Jet Nozzles

Proper jet nozzles are key in effectively delivering grinding fluid. A jet nozzle has a small outlet to increase the coolant velocity. Jets are typically more effective than floods at delivering coolant, and Steffen showed that a more coherent jet provided higher material removal rates [45]. Coherent jets are jets that maintain their shape over a relevant distance, which in grinding may be the distance from the nozzle to the wheel. Webster noted that a coherent jet is more able to effectively deliver coolant by penetrating the air layer and reaching the wheel surface, and also noted that jets can reduce misting [20, 28] which leads to both lower cooling effectiveness and potentially health issues [45].

Shoe Nozzles and Direct Delivery

The shoe nozzle was developed in the 1970s to effectively deliver coolant while avoiding the need for high pumping pressures or penetrating the air layer. The shoe is a diverging nozzle with an opening that conforms to the wheel geometry, which is pressed against the surface of the grinding wheel [9]. With the shoe in place, coolant can be supplied at a low pressure. The voids on the surface of the porous wheel are filled, and the rotation of the wheel acts like a pump to accelerate the fluid and carry it into the grinding zone [7]. The shoe nozzle dispenses with any issues of the air layer, as its geometry scrapes the air from the wheel surface entirely, preventing it from interfering with the coolant. The shoe nozzle is not without its downsides, though. Its positioning relative to the wheel surface must be precise, and concerns over whether its bulk and constant need of readjustment are appropriate for general grinding have been raised [20, 24].

Other Methods of Coolant Application

Other types of coolant application include MQL, needle nozzles, and brushes. In MQL (Minimum Quantity Lubrication), a two-phase mist of coolant and air is directed towards the grinding zone [7]. By using MQL, flow rates can be reduced by a factor of 20,000 [47].

The needle nozzle is comprised of a series of tubes that can be arranged to deliver coolant in specific shapes [24], which is ideal for a contoured workpiece.

Hosokawa developed an innovative low flow delivery mechanism where fluid flows down the surface of brush bristles, or along the inside of hollow bristles, to be deposited on the wheel surface. This avoids the issues of the air layer, allows for ease of application of fluid on irregular profiles, and avoids the positioning issues inherent to the shoe nozzle [21].

2.2.2 The Air Layer

One of the basic principles in fluid mechanics is the no-slip condition, which states that a fluid in contact with a solid surface will have no relative velocity to that surface, due to viscous effects. This leads to the development of a velocity profile between the surface and the free stream fluid, away from the surface. The distance from the surface where the fluid reaches 99% of the free stream velocity is known as the boundary layer thickness, and this region is known as the boundary layer.

In grinding applications, the fast moving wheel drags a significant amount of air on its circumferential surface as a boundary layer [48]. This layer is called alternatively the air layer, barrier, belt, or bond in the literature. The air layer has both tangential and normal components, with the latter being supplied by flow through the sides of the porous wheel that is then expelled at the periphery. Alenius and Johansson [11] state that the magnitude of flow in the normal direction is so small that it can be considered negligible relative to the flow in the tangential direction.

The air layer has two major modes of impact on the delivery of coolants. For coolant that is directed towards the wheel surface, the air layer acts as a crossflow, deflecting and redirecting the coolant away from the grinding zone [19,49]. When the coolant is applied directly into the grinding zone, at an angle almost parallel to the workpiece surface, the air layer changes direction and spouts out, as illustrated by Ebbrell in figure 2.7. This again blocks the coolant from the grinding zone.

Beyond preventing the delivery of the coolant to the grinding zone, the air layer also has the effect of mixing the coolant jet with air, creating (or increasing the gas fraction of) a liquid-gas two phase flow [14]. This two phase flow both has a lower cooling capability in the grinding zone and can result in coolant mist generation,

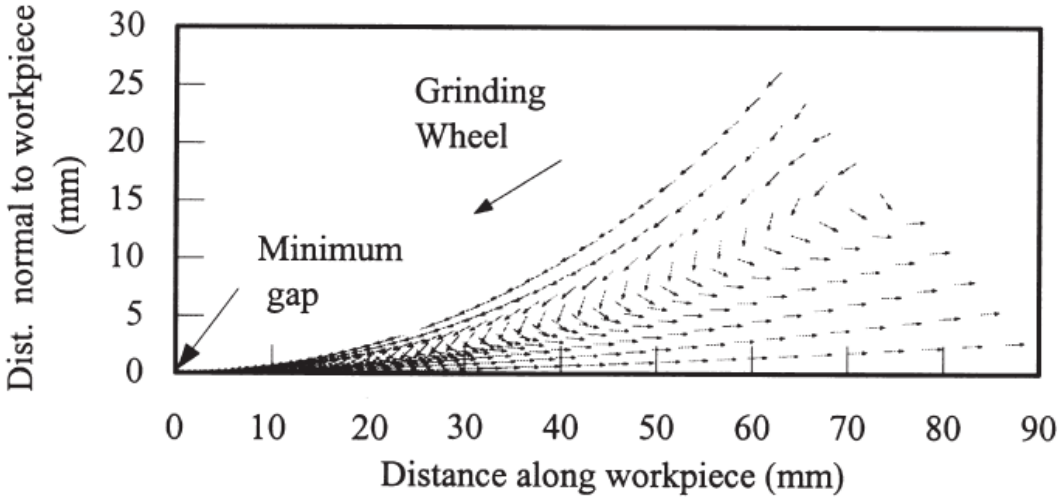

Figure 2.7: Flow field of the air approaching the contact patch [15]

which has negative health impacts for the operator [45].

The jet must have sufficient velocity to overcome the air layer but efforts have also been dedicated to reducing the strength of the air layer, to lessen its impact. A plate can be used to "scrape" the air away from the wheel, which lessens its effect on the coolant [18]. The gap between the wheel surface and the scraper needs to be kept reasonably small, requiring frequent adjustments which are inconvenient in high production industrial settings [50, 51]. The scraper also has to be positioned fairly close to the jet contact point, as the air layer is reported to regenerate after approximately 20° of wheel travel [39].

Strength of the Air Layer

The strength of the air layer is solely a function of its velocity profile. The no-slip condition of a fluid in contact with a solid surface requires the relative velocity to be zero at that surface, but the porosity and 'air spouting' effect of the rapidly spinning wheel may affect the tangential velocity profile as it decays with distance. Knowing the strength of the air layer is critical to overcoming it, as this is the strength that the jet needs to match or exceed. Several researchers [11, 18] have measured this tangential velocity, and some have developed models for the velocity profile.

Trmal and Kaliszer [18] state that the strength of the air layer can be determined by calculating its momentum using the average velocity of said layer and its thickness.

$$M_{\text{air}} = \rho \cdot h_{\text{air}} \cdot \bar{u}_{\text{air}}^2 \tag{2.8}$$

This method may be useful in situations where the velocity can be measured, but the determination of the thickness and average velocity of the air layer is difficult. Boundary layers never clearly end, but rather trail off into the surrounding atmosphere. The thickness of a boundary layer is typically considered to be the point where the velocity reaches 99% of the free stream velocity, or in this case, 1% of the surface speed v_s.

Radhakrishnan and Rahman [12] investigated the air layers generated by grinding wheels of different diameters and grit specifications. They developed an equation to describe the air layer profile, from data collected at radial distances of 0.3-10 mm from the wheel surface.

$$u\left(t\right) = 0.116 v_s^{1.05} \frac{R_t^{0.215}}{t^{0.22}} \tag{2.9}$$

In equation 2.9, the air velocity is a function of the wheel speed v_s, the distance from the surface t (which is in mm), and the wheel surface roughness R_t in µm. The surface roughness is predicted from the wheel grit specification g_s with equation 2.10.

$$R_t = 380.61 - 3.82 g_s + 0.01 {g_s}^2 \tag{2.10}$$

Alenius and Johansson [11] conducted a similar experiment, and found that for a given wheel the dimensionless velocity profile was consistent across different wheel speeds. They fit two curves to the recorded data, one which matches the experimental values from the wheel surface to 14 mm away and the other that fits well from 1 mm from the surface onward. Both are a function of t, the distance from the wheel surface in mm.

$$u' = \begin{cases} 1 - 0.595 \cdot t^{0.17443} & 0 \leq t \leq 14\,\text{mm} \\ 0.44936 \cdot 10^{-0.062849t} & 1\,\text{mm} \leq t \end{cases} \tag{2.11}$$

Alenius and Johansson's profile converges to zero as the distance t increases,which is expected from a boundary layer, while Radhakrishnan's profile does not.

In the model proposed by Trmal and Kaliszer and used by others such as Qiu [52], the thickness of the air layer is the *average air layer thickness*, which is not directly quantified. Trmal and Kaliszer use a pitot tube assembly to measure the profile over the distance between the wheel and the nozzle, which is 5 mm away in that particular case. It is unclear if a different value based on other characteristics of the apparatus can be used. Qiu does not provide details of how the thickness is determined in their work when using this model.

Penetrating the Air Layer

It is commonly held that in order to penetrate the air layer, the jet velocity must meet or exceed the wheel velocity [20, 33]. Cui [53] measured the heat transfer from a simulated grinding heat source to the coolant with a range of jet to wheel velocity ratios and found that the heat flux was highest when the jet velocity matched or exceeded the wheel velocity. Cui also stated that a close velocity ratio would reduce splashing. Several researchers have measured the effective flow rate over a range of jet to wheel velocity ratios [10, 32, 34, 44, 52, 54, 55].

A representative sample of those results are collected in fig. 2.8 where each line

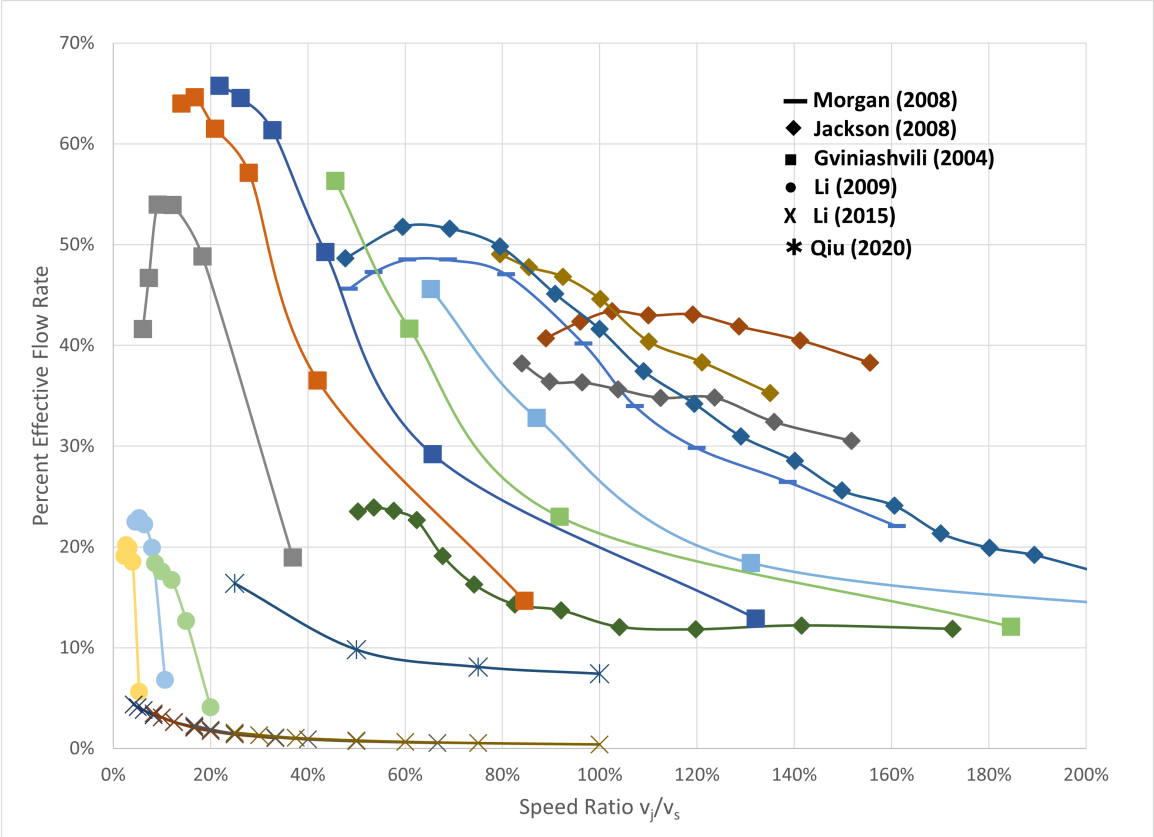

Figure 2.8: Effective flow rates from various sources

represents a set of trials with consistent parameters. Only one trial set, by Gvini-ashvili, shows a maximum effective delivery at a relative speed of 100%. This suggests that matching the jet speed to the wheel speed is not necessarily the only requirement, or the most important consideration to delivering coolant through the air layer and maximizing the effective flow rate.

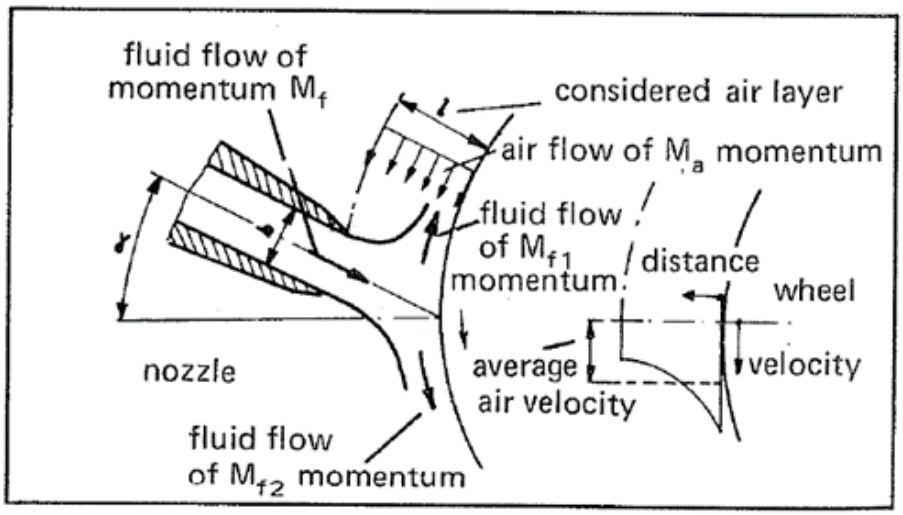

Figure 2.9: Interaction of an inclined jet with the air layer on a grinding wheel [18]

Trmal and Kaliszer [18] applied fluid jets of various velocities to the wheel, and found that the critical velocity required to penetrate the air layer was a function of the relationship between the jet momentum and the air layer momentum. They presented the model shown figure 2.9, with the inequality $M'_j \geq M_{air}$ to predict when the jet would penetrate the air layer and "stick" to the surface of the grinding wheel. Here, M'_j is the per unit width jet momentum that flows "up" the wheel, and M_{air} is

the per unit width air layer momentum.[1]

$$M_j = \rho_j \cdot d_j \cdot v_j^2 \tag{2.12}$$

$$M_j' = M_j \frac{1 - \sin \alpha_\mathrm{n}}{2} \tag{2.13}$$

In this model the jet is split when it hits the wheel, and a portion of it flows up while a portion flows down, as a function of the impact angle. Batchelor [56] conducts a similar analysis of a jet impinging on a flat plate at an angle, and demonstrates that the above modifying factor $\frac{1-\sin \alpha_\mathrm{n}}{2}$ describes the relative liquid layer height that flows up the wheel, and that $\frac{1+\sin \alpha_\mathrm{n}}{2}$ describes the height of the liquid layer flowing down the wheel.

The portion that flows up acts similar to a scraper, opposing the air layer, pushing or scraping it away with its momentum, and allowing the bulk of the jet to wet the wheel surface. Based on Trmal and Kaliszer's analysis, a jet that impacts the wheel at an angle normal to the wheel surface would need a lower velocity to penetrate the air layer than one with a higher impact angle α_n.

Akiyama performed a similar experiment where a jet of coolant was applied to the surface of a wheel at a range of angles, and the thickness of the fluid film in the grinding zone was measured. They found that jets that hit the wheel surface at angles closer to normal resulted in thicker coolant films, which would agree with Trmal and Kaliszer's analysis [14].

Inasaki [16] investigated a jet of coolant directed parallel to the workpiece into

[1] Trmal and Kaliszer use a different notation than the one used in this work. Here h_air, M_j', M_{air}, and d_j are used in place of l, M_f1, M_a, and b, respectively.

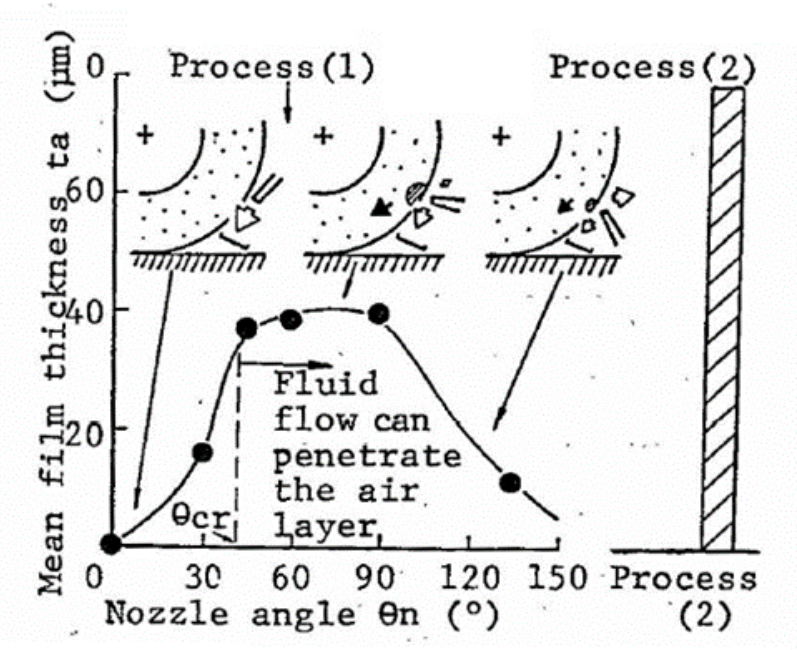

Figure 2.10: Height of coolant film on the wheel surface at (1) different nozzle orientations and (2) with flow forced into the grinding zone [14]

the converging wedge. He found that there is a critical jet velocity required to reach the grinding contact, opposing the recirculating air in that region.

2.2.3 The Coherent Jet

The results presented by Inasaki, Akiyama et al, and Trmal and Kaliszer above show that the velocity of the jet when it reaches the grinding wheel as well as the direction in which the jet is oriented are critical to effectively penetrate the air and deliver grinding coolant. Jets of fluid in any medium have the tendency to break up over time. A coherent jet is one that produces a consistent stream of fluid that maintains its shape and does not increase in diameter or entrain air as the distance from the nozzle increases. This is critical, because as a jet diverges from its original diameter, it either entrains air or undergoes a reduction in average velocity, in order to maintain conservation of mass. Either of these will result in lower mass and momentum fluxes across the jet's cross sectional area, which has a negative impact on both air layer penetration and general cooling ability.

There are a variety of terms used around coherent jets, with research groups describing the concept differently, including *coherent*, *coherency*, and *the coherence length*. Formally, a jet is considered to be coherent until the height of the surface waves equals the initial radius of the jet [57] via [58].

Since surface waves typically do not appear as perfect sinusoids in nature, this definition has limited practical value. Webster [28] defines a coherent jet as one with a diameter less than 2 - 3 times the nozzle diameter at a distance of 12 inches. Baines-Jones [59,60] uses the existence of a velocity core to define the coherent jet, and assumes that when the width of the core diminishes to zero, the jet loses coherence. In both these cases, the coherence length is the distance where this coherence condition is met. Geilert [61] states that it is the length at which fluid atomization begins.

Other works dismiss the idea of a binary of jet coherence or incoherence - and with

it a specific coherence length - and instead consider the idea of coherency which is the degree to which a jet has dispersed. Warkentin [62], St-Pierre [63], Irani [64], and Steffen [45] use the ratio of the jet diameter to the nozzle diameter at various distances downstream, and use that definition to compare jets to one another. Rouly et al [65] determined the angle of divergence of the jet for their measurement of coherency, and in their elliptical jet measured it along both the major and minor axes.

Measurements of Jet Coherence

To measure jet coherence, coherence length, and breakup, researchers have used three primary methods. Cui [53] used a caliper system, where the upper and lower extents of the jet were measured at several points along the jet length by touching a sharp probe to the liquid surface. Cui reported a resolution of 0.05 mm and an uncertainty below 4%. It is unclear if a visual inspection was depended on to determine when the caliper contacted the jet, or if some other method was used.

Baines-Jones [59, 60] used a pitot tube technique, where a small tube, oriented normal to the jet velocity, was passed through the jet along the diameter. The stagnation pressure was measured, and converted to velocity. Through this method, Baines-Jones was able to determine the jet diameter, the velocity profile, and the length of the jet's initial velocity core. Similarly, Geilert et al. [61] passed a jet over a force sensor with a 1 mm target, which allowed them to map the shape of the jet as well as its momentum.

Several researchers [42, 61, 63, 65–67] used imaging techniques to determine the spread of the jet over a distance. Rouly et al. [65] took still, high quality digital photos of the jet and measured the angle of the jet spread. Similarly, St-Pierre et al. [63] took still photos of the jet at a series of discrete stand off distances, and

calculated the "jet opening ratio" or jet coherency, based on the measured diameter. In both cases, the shutter speed does not appear to have been set to obtain clear, instantaneous images but instead provided a time averaged shape.

Other researchers used high speed imaging techniques to look at the instantaneous shape of the jet. Hoyt et al. [66] set up a film camera, and ran the film behind the lens at a speed matching the jet that they were imaging. When the jet was in the center of the film, a 15 µs diffuse flash was activated to capture the image. Since the film was moving at the same speed as the subject, they were able to use long exposure times compared to the short exposure times used in later works. Nguyen et al. [67] used a similar stroboscopic method, where the jet was illuminated for a very short duration (<3 µs) to achieve a clear image. Geilert et al. [61] and Heinzel et al. [42] used high speed cameras for this purpose. Geilert describes an apparatus in which the jet was backlit through a translucent glass plate to achieve even illumination. They also reported that an exposure time of 1/60 000s was effective in obtaining a high-quality image of the 35 m/s jet surface.

Generation of a Coherent Jet

There have been several methods used to generate coherent jets, with varying degrees of efficacy. Use of any particular method, or multiple methods in parallel, will be constrained by process requirements, pumping capacity, and space limitations.

Nozzles

Much work and investigation has been done on the topic of nozzle design. Webster is considered one of the first researchers to investigate coherent jets for grinding [25], and designed two nozzles, one round and one planar, with concave contractions, to reduce boundary layer growth and prevent flow separation. Webster compared the jet coherence of the planar nozzle at a distance 30.5 cm to a commercially available rectangular nozzle, reporting significant improvement over a range of Reynolds numbers [20]. Webster states that critical considerations to jet coherence in nozzle design include the nozzle's interior surface quality, the contraction ratio, and ensuring a sharp nozzle exit.

Cui [53] confirms the need for the nozzle to have a concave contraction. Others speak only of the need for transitions to be smooth and continuous. Rouse states that any sharp angles in the nozzle contraction can lead to eddies and add turbulence to the flow [68] via [69]. McCarthy and Molloy claim that there aren't any qualifications on how to shape the curve of a nozzle beyond it being smooth and "pleasing to the eye" [69]. Lopez-Arraiza et al designed a nozzle using CFD, and compared it to the work of Webster in an experimental setup. They found that custom designed curves produced a higher quality jet, and resulted in lower energy consumption due to reduced flow losses [19]. Rouly et al attempted to make elliptical jets with customizable divergence angles [65]; they found success in being able to effectively shape the jets using 4^{th}

order Bezier curves, although it is unclear if the jets had a desirable jet surface quality.

In terms of the nozzle's surface quality, there has been some debate. Rouse claims that the surface roughness is not particularly important, assuming that there aren't any major burrs or imperfections [68] via [69]. McCarthy and Molloy [69] and Cui [53] disagree, and state that a polished internal nozzle surface will have a much higher coherence than an unpolished alternative. Cui attributes this effect to the unpolished surface acting as a turbulence generator. Hoyt and Taylor observed striations in the axial direction along the jet surface as it left the nozzle, and attributed them to near invisible imperfections on the nozzle surface [70].

The final component that receives much focus is the nozzle exit, of which both the exit length and the exit shape have been discussed. Historically, nozzles have had long exit lengths, in order to protect the nozzle from damage [53]. Rouse states that the length of the exit after the contraction should be as short as possible [68] via [69]. McCarthy and Molloy demonstrated that a smaller exit aspect ratio (the ratio of the exit length to exit diameter) had a beneficial impact on breakup length [69]. Cui explained that a large aspect ratio will result in the exit behaving like a straight pipe, generating eddies and secondary flows. His work showed that a nozzle with an abrupt exit following the contraction performed significantly better than a one with a tip, which was little better than a piece of pipe [53]. This conclusion is in line with that of Hoyt and Taylor, who recommended that a tip not be used if it wasn't needed [70].

Regarding the exit shape, Cui found that the edge of the nozzle exit had a major impact on the jet quality as well. He states that the exit edge must be sharp, without a chamfer or radius, in order to get a clean jet surface, as having either could result in flow separation [53]. Baines-Jones confirms this, saying that a nozzle should have

a sharp exit, and be free of nicks and burrs [58].

The contraction ratio β, which is the ratio of the nozzle diameter to the upstream pipe diameter, and is defined in equation 2.16, has been shown to have an effect on the jet coherence. Cui reported that a lower contraction ratio will improve jet coherence, and that a straight pipe will generate the least coherent jet [53]. Hoyt and Taylor observed that lower contraction ratios can reduce nozzle spray [70]. McCarthy and Malloy state that the flow from the nozzle is a direct function of the upstream flow, so for constant jet velocities a higher contraction ratio means that the upstream flow had a lower Reynolds number and turbulence [69]. Cui, however, attributes these results to the relaminarization process where the turbulent layers are compressed as the flow area decreases [53]. In their work on wind tunnels, Bell and Mehta state that a contraction reduces turbulence in both the axial and radial directions [83]. Overall, the contraction can be seen to have a significant impact on the jet coherence and quality.

Irani et al [71] and Mandanchi et al [24] summarized - from previous works - the common design criteria that should be followed to achieve a coherent jet from a nozzle. Their lists can be combined as:

- The nozzle outlet must be sharp, not rounded
- The internal surface must have a smooth finish
- There should be a high level of contraction from the inlet to the outlet, and the transitions should be smooth, concave or parabolic, and have angles above 7 degrees
- The nozzle should have an abrupt exit

Hydraulic Flip

In converging or sudden contraction nozzles, the fluid separates from the sides of the pipe or channel at the upstream edge, or lip of the nozzle. In low velocity conditions, the flow can reattach to the downstream sides of the nozzle and spread back out to fill the nozzle. Reattachment disturbs the flow's uniformity, and the flow does not leave the nozzle as a coherent jet.

At a certain critical flow rate, the point of reattachment will be at the exit of the nozzle, and the jet leaves the nozzle maintaining its coherence. This abrupt transition to a coherent jet has been called *hydraulic flip*.

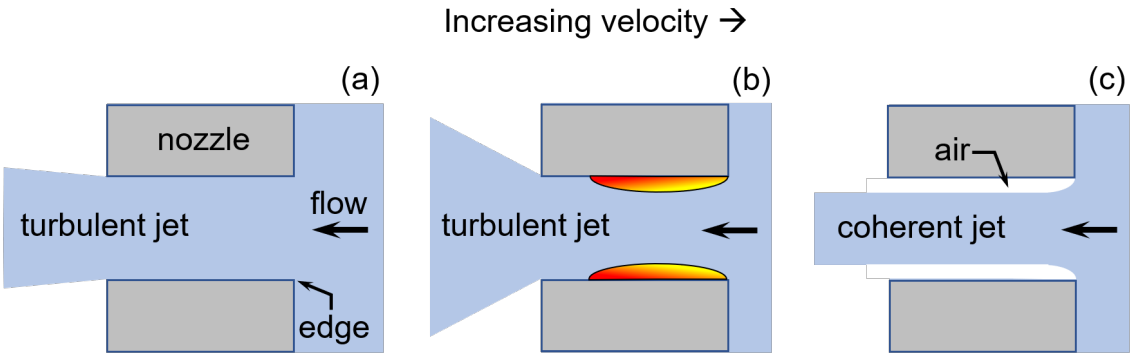

Figure 2.11: Stages of hydraulic flip

Iciek describes the situation as one where the jet is no longer wetting the nozzle walls, which would mean that surface roughness, among other things, is no longer a factor. The resultant jet is more stable, without breakup mechanisms such as surface waves [78], and has been described as smooth and having a "considerable increase of the breakup length" [77]. Both Chew [79] and Iciek [77] described a hysteresis effect where the system pressure (or system flow rate) could be reduced below the critical value that was required to achieve the hydraulic flip, without rewetting the nozzle wall. As a result, the high quality jet can be achieved at lower velocities than the

critical velocity. Eventually the flow reaches a point where the jet contacts the nozzle walls, partially and then fully wetting them, destroying the jet coherence.

The separation of the flow from the upper lip of the nozzle produces a coherent jet with a diameter smaller than the nozzle opening. The flipped jet then has an actual velocity higher than a nominal velocity based on the flow rate and nozzle area.

The ratio of the area of the jet to the area of the nozzle is called the contraction coefficient, and is defined in equation 2.14, where A_j is the jet area, and A_n is the nozzle area [81].

$$C_C \equiv \frac{A_j}{A_n} \tag{2.14}$$

Several works present values for C_C. Batchelor states that the coefficient can range from 0.5 to 1 for the vast majority of orifices, and that for a simple hole in a flat surface, the contraction coefficient will be between 0.61 and 0.64 [56]. Baines-Jones states that this value is typically 0.63 [59], while Lienhard and Lienhard reported the well known relationship, presented in equation 2.15 [82].

$$C_C = \frac{\pi}{\pi + 2} = 0.611 \tag{2.15}$$

Benedict et al, in their 1966 work [81], analysed velocity independent measurements taken in earlier studies, and presented a least-squares regression of the contraction coefficient as a function of the contraction ratio β. If β can be defined by equation 2.16, then the contraction coefficient may be calculated with equation 2.17:

$$\beta = \frac{d_{nozzle}}{d_{pipe}} \tag{2.16}$$

$$C_C = 0.61375 + 0.13318\beta^2 - 0.26095\beta^4 + 0.51146\beta^6 \tag{2.17}$$

The resultant curve is plotted in fig. 2.12. One can note that for nozzles considerably smaller than the flow delivery pipe (in other words, a low β value), the previously noted values of around 0.6 are seen.

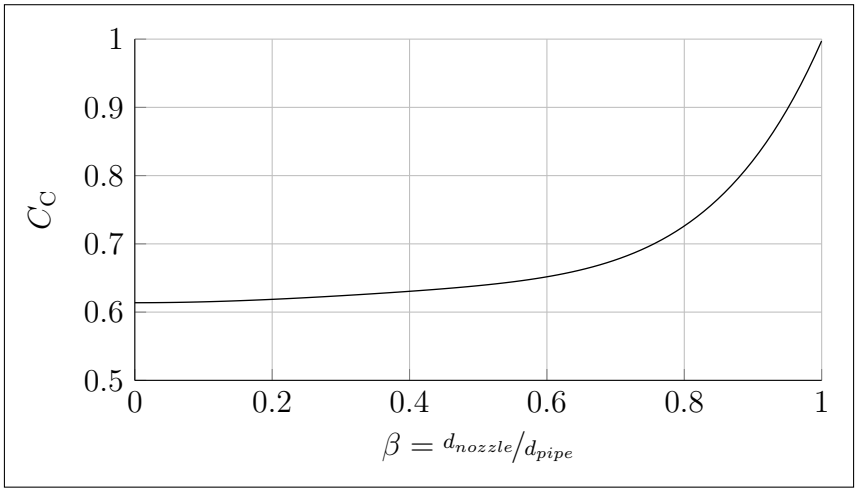

Figure 2.12: Contraction coefficient as a function of contraction ratio β

Flow Conditioners

A flow conditioner is a device that allows one to generate a desired flow pattern [53]. In a piping system, boundary layers, fittings, and imperfections give rise to turbulent and undesirable flow patterns, including irregular velocity profiles and secondary flows or swirl [20]. McCarthy and Molloy [69] describe the impact that a non-uniform profile can have on the jet quality, and the instabilities (including surface waves) that arise from a non-uniform profile transitioning to a uniform profile as the jet leaves the nozzle. They state that an incoming flow with a plug profile will result in a much more stable jet. Here we refer to flow conditioners in the most traditional sense, as a means to remove these undesirable patterns and generate a uniform flow profile [72].

The need for a flow conditioner can be reduced by controlling the conditions at the inlet to the nozzle. In their 1966 work, Grant and Middleman [57] took care to reduce perturbations and disturbances by controlling expansions, contractions, and fittings. Rouly et al. [65] used rubber tubing set in large radius curves to replace short pipe and elbow attachments, and ensured that there was a section of straight pipe ahead of the nozzle. Webster et al. [20] demonstrated that a long straight pipe placed between the elbows of a coolant supply system had a similar effect to a flow conditioner installed in the same location. Webster qualifies this by stating that the length of the pipe required to get the desired effect (48 times the pipe diameter) would make using this technique in real world grinding applications impractical.

There are two primary categories of flow conditioners, depending on their function. The first is primarily intended to eliminate swirl and transverse motion, and the second to create a desired velocity profile. Baines-Jones [59] splits this second category

into two further types, differentiating between the creation of an axisymmetric profile and the creation of a uniform or otherwise desirable velocity profile.

The first category of flow conditioner, often referred to as a 'flow straightener' in industry, is typically a series of straightening vanes or honeycomb. It reduces swirl by forcing the flow through parallel channels, removing eddies. Some researchers [59, 73] state that conditioners in this class do not have an effect on the flow velocity profile, but others [45, 53] show improvements to the velocity profile after the use of this style of conditioner as would be expected due to the pressure drop across the channels.

Honeycombs can also reduce turbulence levels sufficiently to provide laminar flow. In order to do that, the diameter of the channels must be small enough that the Reynolds number (based on the channel diameter D) is within the laminar regime, or below 2300. The channel length also needs to be long enough for the development of a laminar profile. Cengel and Cimbala present equation 2.18 for a fully developed flow, as a function of the channel diameter D and Re_D [74].

$$L_{\text{dev}} \approx 0.05D\frac{\rho\bar{u}D}{\mu} = 0.05D\ Re_D \tag{2.18}$$

The second category of flow conditioner provides a specific velocity profile, for which a uniform resistance, fine mesh, or perforated plate is used. Compared to the first category, this type of conditioner has less impact on swirl [73], but redistributes the flow into an even profile. As mentioned above, Baines-Jones differentiates between conditioners that create a uniform plug profile and those that create a more specific velocity profile. An example of the first is a simple mesh of unifom resistance, and of the second a perforated plate with a controlled orifice pattern.

The degree to which the velocity profile of a particular case differs from a uniform

profile can be said to be equal to the kinetic energy coefficient ε [72], also known as the energy defect ratio or the velocity profile factor. The kinetic energy coefficient is calculated from equation 2.19, where u is the velocity as a function of position, $\bar{u}$ is the average velocity, and A is the cross sectional area of the jet [69].

$$\varepsilon = \frac{\int_A u^3 \, \mathrm{d}A}{\bar{u}^3 A} \tag{2.19}$$

A perfect plug flow, or in other words a uniform velocity profile, would have $\varepsilon = 1$, which is the lowest possible value. Fully developed turbulent pipe flow can be said to have a value of $\varepsilon = 1.1 \sim 1.2$, and the parabolic profile of a fully developed laminar flow would have a value of $\varepsilon = 2.0$ [69]. The closer ε is to 1.0, the more stable the resulting jet will be.

A flow of any profile will have an average velocity and a maximum velocity. For a flow passing through a uniform resistance with an initial kinetic energy coefficient ε_1 and velocities $\bar{u}$ and $u_{1,max}$, the maximum velocity after the resistance can be calculated with equation 2.20 [72]. The pressure drop coefficient K is defined in equation 2.21, and is the ratio of the difference in static pressure to the dynamic pressure [75].

$$\frac{u_{2,max}}{\bar{u}} = \sqrt{\frac{(\frac{u_{1,max}}{\bar{u}})^2 + \varepsilon_2 - \varepsilon_1 + \varepsilon_2 K}{1 + K}} \tag{2.20}$$

$$K \equiv \frac{p_2 - p_1}{\frac{1}{2}\rho \bar{u}^2} \tag{2.21}$$

These equations show that a higher resistance will more greatly redistribute the flow towards uniformity.

The "Mitsubishi" conditioner is frequently used in the literature, and consists of

a simple disk with holes drilled along concentric circles [45, 53]. An adjustment was made to this conditioner by Cui, changing the diameter of the holes to ensure that each concentric circle would have a consistent liquid flux. This was shown to provide a slightly better jet coherence in systems with small nozzle lengths. Baines-Jones [59] describes the original Mitsubishi conditioner as a flow straightener, and the adjusted version as one able to create the uniform plug profile.

Equipment used to condition flows and develop velocity profiles can be added together in series, which overlays their effects upon one another. Applying honeycombs, uniform resistances, and flow conditioners to the same flow leads to significant decreases in eddies and flow instabilities. Certain combinations can also negate negative effects of each component. Loehrke and Nagib showed that while a honeycomb develops a flow into the laminar regime, it also generates a significant turbulent wake when the individual streams recombine. Though screens should typically be used ahead of a honeycomb to even the velocity distribution, the addition of a screen after the honeycomb removes this added turbulence, while adding only high frequency turbulence that quickly dissipates [75].

Polymer Addition

The addition of a polymer to the working fluid to increase coherence has been the subject of considerable investigation by researchers. Hoyt et al [66] looked at the impact of adding a range of polymer concentrations to the fluid and found that at low concentrations (10 ppm of polyethylene oxide, PEO), the glassy, coherent region directly after the nozzle disappears. They posit that this can be attributed to the fluid mixture either having a lower development length or transitioning to turbulence more readily. At higher PEO concentrations (above 50 ppm), nozzle spray ceased and the jet remained intact for a longer distance. The transparent region reappeared at concentrations above 200 ppm of PEO. Since the addition of the PEO changed both the surface tension and the liquid viscosity, the authors compared the jets with the added polymer to a jet to which a surfactant had been added to change the surface tension appropriately and found that the change in surface tension didn't impact the jet quality. Hoyt and Taylor conducted a similar experiment, adding 200 ppm of PEO to water jets, and observed an overall increase of jet quality and reduction of spray formation. They noted that the jet breakup occurred at the same distance as for pure water [70], however Feng observed both an increased jet quality and a longer coherence length [84]. Hoyt et al showed that the addition of polymers reduces small scale variations and surface waves, but has no effect on large scale motion or jet oscillations [66]. Wijk, on the other hand, observed that while the polymer increased jet coherence, it also increased jet oscillation [85]. Feng et al [84] and Hoyt et al [66] attribute the stabilizing effects of dissolved polymers to an increase in viscosity, and Feng et al [84] and Hoyt and Taylor [70] include the idea that polymers reduce the internal drag of the fluid flow and can thin the turbulent boundary layer.

2.3 Summary of the Literature Review

Coolant is critical in grinding processes, and ineffective coolant application will have a significant impact on manufacturing outcomes, affecting productivity, dimensional tolerance, and surface quality. The primary obstacle that must be overcome is getting grinding fluids into the space between the wheel and the workpiece, but the air layer and other complexities of the grinding process make this difficult.

Penetrating the air layer has been the focus of a plurality of this review. The structure and strength of the air layer was considered, as were the two competing ideas of how best to traverse it. The best method for coolant delivery in high-speed grinding, based on flexibility and the depth of research conducted, is through the use of free, coherent jets. These jets maintain their shape and their momentum and can both be accurately aimed and effectively penetrate the air layer or the reversing air flow. Different methods of generating a coherent jet were reported, as was the principle that the methods can be combined with synergistic effects.

Currently used techniques to create a high-speed coherent jet leave much to be desired. The state of the art includes jets that quickly diverge, or which have significant surface waves and air entrainment. There is much room for improvement, which will be the focus of this work.

Chapter 3

Experimental

The objective of this experimental work is to develop a truly coherent jet and to characterize the efficacy of the coherent jet relative to what has been considered to provide the most effective commercially available coherent jet – the Rouse nozzle. These experiments start with the development of a nozzle that generates a coherent jet, and compare the developed jet to the jet issuing from the Rouse nozzle through optical and mechanical coherence measurements, air layer penetration experiments, and direct grinding trials to compare the effectiveness in terms of heat control.

The primary objective of coolant in grinding is to facilitate high productivity through effective management of waste heat. Subsequently, the ultimate measure of the quality of a cooling jet is to determine the manufacturing productivity that it permits. The development of the high quality nozzle and the experimental procedures used are detailed in this chapter.

3.1 Design of a Flow Conditioner

Several different styles of flow conditioners have been used in previous works, which have contributed to increased jet coherence and a longer breakup length. A large portion of the present work was dedicated to the development and characterization of a coherent coolant jet that can be used in real world grinding processes. To achieve this coherent jet, a flow conditioner was developed with the design objectives of reducing or eliminating turbulence in both radial and axial directions and removing velocity variations. Conditioning the flow completely before the nozzle, and using a sharp and abrupt nozzle transition, means that the complicated nozzle design that had been focused on in previous works may be dispensed with entirely.

Initial design requirements were the ability to supply approximately 25 L/min at a nominal[1] jet velocity of 30 m/s. The literature puts a special emphasis on matching the velocity of the jet to the surface speed of the wheel, which typically is around 30 m/s. A ¾ NPT inlet was chosen for convenience in attaching the conditioner to test machinery. Aside from these static requirements, the problem was open beyond the objective of generating a coherent jet.

It is difficult to know the quality of a flow coming into a nozzle. The expected velocity profile for flow under turbulent conditions (which a standard flow rate and nozzle diameter would have) is that of a largely uniform flow (also known as plug flow), but upstream conditions such as valves and bends can change the profile in unexpected ways. As such, no simplifying assumptions could be made about the inputs to the flow conditioner beyond its volumetric flow rate and the inlet diameter.

[1]By nominal we mean the velocity calculated by dividing the volumetric flow rate by the nozzle area. This is not the true jet velocity, as there is profile relaxation, surface waves, and jet area changes due to the hydraulic flip.

To allow for the highest opportunity for success, the worst-case input conditions were assumed: a fully turbulent flow with a significant radial, non-axisymmetric velocity profile, and low frequency, long wavelength eddies. The flow conditioner can be considered to have four primary segments, each dealing with a different aspect of the flow that would be detrimental to jet quality.

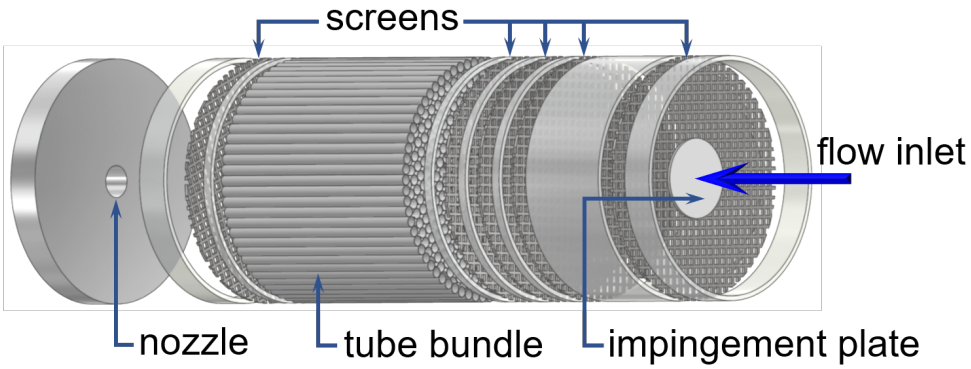

Fig. 3. Exploded view of the flow laminarizing device.

Figure 3.1: Exploded view of the developed conditioner

The first region, which in fig. 3.1 is the area between the flow inlet and the tube bundle, deals with the bulk velocity profile. The flow entering at the inlet strikes an impingement plate that has a diameter slightly larger than the inlet pipe. This directs the flow out and around it, breaking up the flow and ensuring that it spreads across the cross-section of the conditioner. The flow then passes through a metal mesh screen (16 x 16 304 steel mesh made of 0.7 mm diameter wire), which provides a uniform resistance and pressure drop, before entering a settling plenum. After the flow has had the opportunity to settle slightly, it passes through three additional screens in quick succession. The screens are used to even out the velocity distribution and bring the velocity profile factor ε as close to 1.0 as possible. Screens were used instead

of perforated plates because they allowed for the benefits of both the Mitsubishi conditioner (ease of manufacture) and the Cui variant (consistent mass flux across the radius). Since the screens have negligible depth, their flow straightening effects would be minimal (but not zero, according to the literature [86]). However, this will be addressed by the honeycomb. The short distance between the screens and the honeycomb prevents the growth of boundary layers which would effect the velocity profile. After this region, the flow velocity has a flat profile; however, it remains turbulent with flow eddies and long wavelength perturbations.

The second region is comprised of the honeycomb, the purpose of which is to develop the flow into the laminar regime and remove any radial or rotational flow that may remain. The Reynolds number Re_D is well known in fluid mechanics, defining the regime of the flow. For an internal flow, the characteristics of the fluid that enters a pipe or a channel are preserved until the boundary layer generated by the walls of the pipe grows to fill the area of the channel. The process of boundary layer growth is known as developing flow, and once the boundary layers have filled the area and combined, the flow is considered "fully developed". The objective for a coherent jet is to have a laminar flow, which is predicted by a Re_D lower than 2300 [74]. The Re_D is calculated with equation 3.1, where ρ is the density, $\bar{u}$ is the average velocity, D is the diameter of the channel, and μ is the dynamic viscosity.

$$Re_D \equiv \frac{\rho \bar{u} D}{\mu} \tag{3.1}$$

To achieve a fully developed laminar flow, the channels must be at least as long

as the minimum development length, repeated as equation 3.2.

$$L_{\text{dev}} \approx 0.05D\ Re_D \tag{3.2}$$

Plastic drinking straws were deemed ideal for the use in the honeycomb due to their small diameter (3.3 mm) which provides a low Re_D, thin walls which allow for maximising the flow area, and smooth surfaces which would prevent them from adding more turbulence to the flow. The velocity of the flow inside the honeycomb is determined by the overall area of the flow conditioner, for which a cylinder with a 70 mm internal diameter was used. This internal diameter results in, for a 25 L/min flow, a velocity of 0.11 m/s. At that velocity, the honeycomb Reynolds number is 401 which is well within the laminar regime. The development length for these conditions, which is the minimum length that the honeycomb may be, is calculated to be 8 cm. An engineering factor was added to this value, to ensure that higher velocities could be handled, and that changes to the density and viscosity of the fluid due to thermal effects would not cause issues. In the end, a 15 cm long honeycomb was used.

Leaving the honeycomb region, the flow from each cell is fully in the laminar regime and has the parabolic profile of an internal laminar flow. The third region of the flow conditioner recombines the multitude of flows into a single plug and passes the flow through a final metal mesh. The addition of the mesh is done to prevent turbulence generated by the recombining flow, shown to be effective by Loehrke and Nagib [75]. The flow at this point is laminar, free of eddies, and has a flat velocity profile.

The final region is the nozzle: The velocity and flow rate requirements set out for the system would require a nozzle with a maximum area of 13.9 mm^2, or a radius of 2.1

mm. A simple aluminum disk of width 10 mm and diameter 70 mm was constructed, with a precision reamed 4 mm exit.

The jet that issues from this developed conditioner seems to be completely coherent at realistic flow rates and stand-off distances. Looking at figure 3.2, the appearance of the jet is similar to that of a glass rod, with a smooth, unperturbed surface and a fully transparent core. It is even possible to clearly read letters through it, although they are refracted and flipped. If hydraulic flip is not accounted for, the pictured jet has a Reynolds number of nearly 45000. Accounting for hydraulic flip and the 3.2 mm jet diameter, that value is over 58000. This would appear to repudiate Vitts' and Otts' statement, relayed by Madanchi et al, that coherent jets are impossible to generate [24].

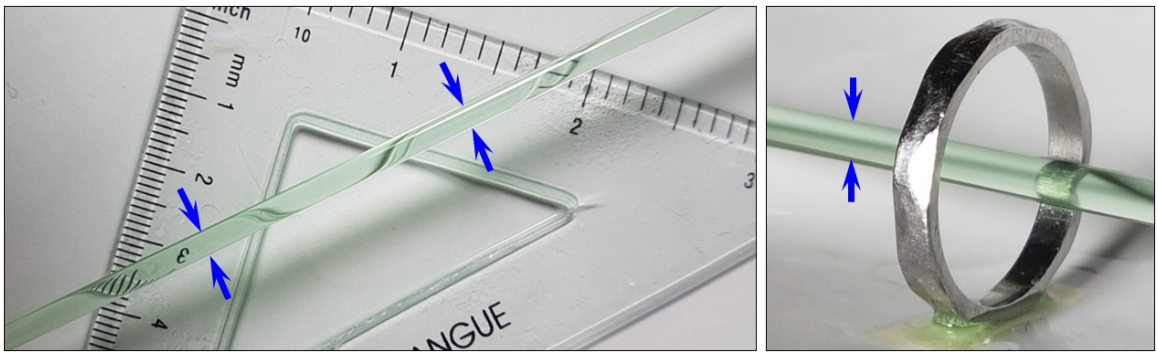

Figure 3.2: Jet issuing from flow conditioner (7.5 L/min, 30 cm standoff)

3.2 Jet Structural Characteristics

While an imperfect definition, a jet typically is considered to be coherent until the jet has a diameter twice that of the nozzle. This combines the original definition by Grant and Middleman with the more modern definitions of Webster, to provide a simple objective for the development of a coherent jet. Coherency, as discussed in section 2.2.3 and described by equation 3.3 below, is used to compare jets at various flow rates and distances.

$$\Xi = \frac{d_{jet}}{d_{jet,nozzle}} \tag{3.3}$$

3.2.1 Dispersion

In order to examine jet coherence, high speed photos of the jets at different flow rates/velocities, for a range of stand off distances were taken. The ChipBlatster J8 1000 high pressure coolant delivery system with a maximum flow rate of 30 liters per minute was used so that a wide range of experimental conditions could be explored. In order to determine an appropriate range of experimental velocities, the coherency of jets from the developed conditioner and nozzle were tracked at 30 cm stand-off as the flow rate was increased. When the coherency, as calculated by eqn. 3.3, was equal to 2, the jet velocity was recorded and a range of velocities from zero to that value were chosen. The experimental conditions are listed below in table 3.1.

A Photron FASTCAM SA-Z high speed camera was attached to a linear stage, able to move parallel to the jet path. The distance between the jet and the camera lens was maintained between trials, so the captured jet diameter with the unit of “pixel

count" could be compared directly against itself without having to be converted to SI units, a conversion that could introduce errors. The jet was backlit, as was done in earlier investigations [61], and a shutter speed of 1/160000s was found to provide a good balance between image clarity and brightness. Images were recorded with Photron's proprietary PFV [Photron FASTCAM Viewer] software, with a total of 500 frames taken at 2000 frames per second. Each recording therefore covers a period of 0.25 seconds and spatial sample of the jet ranging from 1.25 m in the 5 $^{m}/_{s}$ case to 12.5 m in the 50 $^{m}/_{s}$ case.

Table 3.1: Experimental conditions for jet divergence test

Characteristic	Conditions
Nozzles	Developed conditioner 4 mm Rouse nozzle
Jet Velocities	5 $^{m}/_{s}$, 10 $^{m}/_{s}$, 20 $^{m}/_{s}$, 35 $^{m}/_{s}$, 50 $^{m}/_{s}$
Distance away from the nozzle	0[2]cm, 15 cm, 30 cm, 45 cm, 60 cm

The resulting images were analyzed with a purpose-built program, written in MATLAB. The software, which utilized the image processing toolbox, determined the distribution of the jet over time by detecting the upper and lower extents of the jet in each frame using edge detection. The area between the edges is filled in, and the resulting frame is taken as a black and white image matrix, where 1 denotes a filled pixel and 0 an empty pixel.

The values along a central vertical line are taken as an array, and the center of mass of the array is determined. The data is then shifted to have its center of mass in the center of the array, and the values are added to those from previous frames.

[2]Due to the construction of the flow conditioner, there is approximately 5.5 cm between the nozzle and the exit from the contraption where the jet can be imaged. As a result, the images, while reported as being recorded at 0 cm, are recorded slightly downstream. This discrepancy is not carried forward.

The combined values of these frames show the "time averaged density" of the jet along its radius, which can be interpreted as a measurement of the jet's coherence. The center of mass processing was applied to account for pressure inconsistencies in the fluid supply.

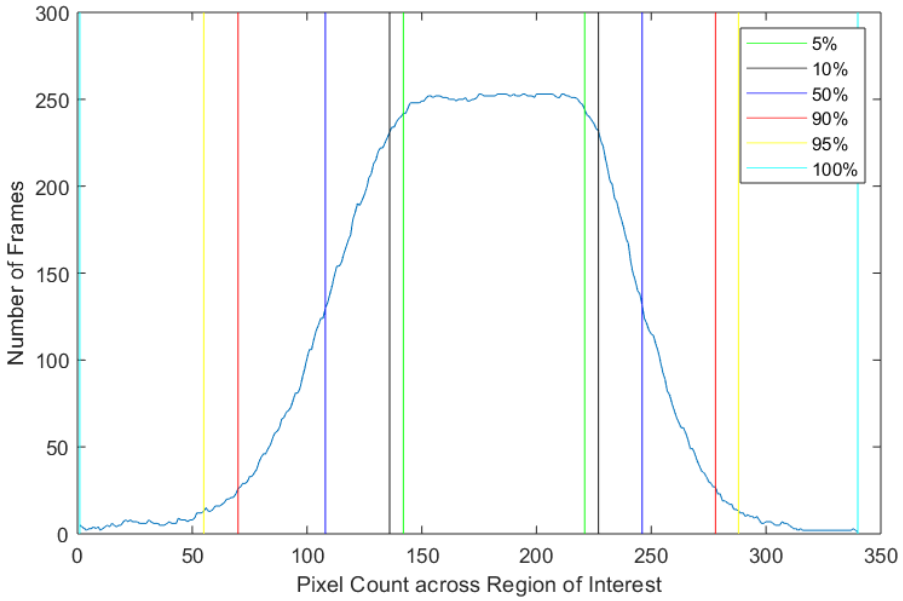

Figure 3.3: Example of the time averaged velocity distribution, for an experiment with 255 frames

The measurements of this "time averaged density" may be plotted as done in figure 3.3. Above, the furthest extents of the jet waves were used to select a maximum velocity for the experimental conditions. This is broadly in line with the formal definition, which considers a jet to lose coherence when the height of the surface wave reaches the value of the nozzle radius. To preserve that standard while avoiding outliers, diameter of the jet that 95% of frames fall within, i.e. a diameter greater than or equal to that of the jet in 475 out of 500 frames is used.

3.2.2 Momentum Fluxes

As discussed in section 2.2.2, the critical condition reported by literature for a jet to penetrate an air layer is matching the per unit width momentum flux (equation 2.13). In the above section, the degree to which the jet dispersed or remained coherent was measured with high speed camera images. This provides a good qualitative understanding of the spread of jets, and limited quantitative understanding through image processing. A direct measurement of the momentum flux and the shape of the jet was desired.

To determine the degree of dispersion of the jet over a distance, a 4 mm wide target (equal to the nozzle diameter) was attached to a Kistler CompactDyn 9254 dynamometer, to measure the impact force of the jet. The developed conditioner and

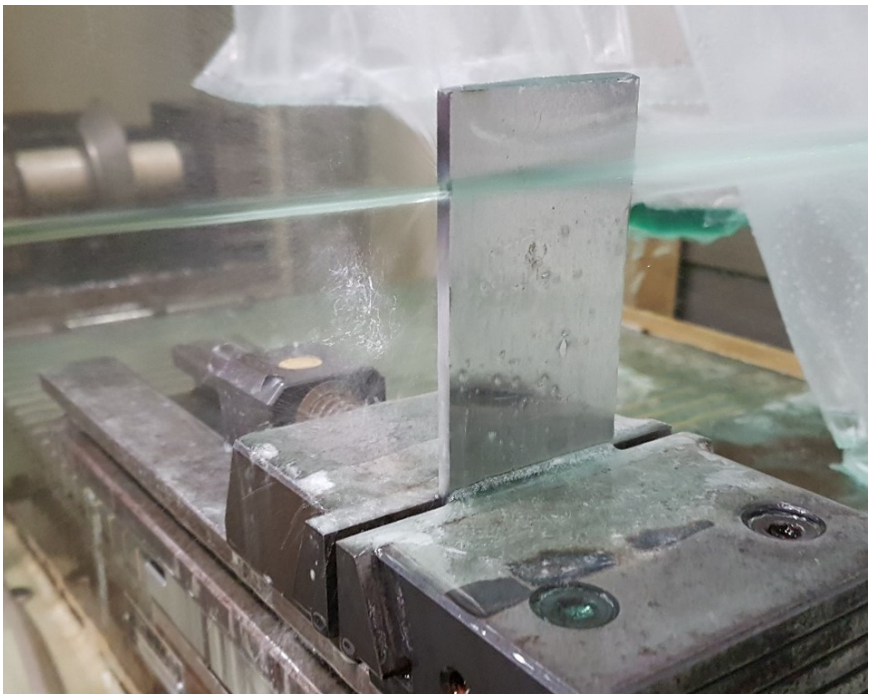

Figure 3.4: Jet striking 4 mm wide target

Rouse nozzle were secured in turn at the experimental distance, orthogonal to the target, and a 7.5 L/min jet was generated. Trials were performed at standoffs of 7, 30, and 60 centimeters. In each case, the flow rate was increased to be above the transition point for hydraulic flip and then reduced to the experimental rate, taking advantage of the increased coherence and the hysteresis effect. The target and sensor were mounted to a motorized linear stage and were passed through the jet spray at a constant velocity of 20 mm/s.

The resultant data was recorded with DynoWare, a proprietary software from the dynamometer manufacturer. The data showed a significant amount of both high frequency noise and drift, which were removed with smoothing and drift compensation tools supplied in the software.

3.3 Penetration of the Air Layer

A series of experiments were undertaken to determine the velocities needed to penetrate the air layer, and to confirm the predictions made by various models. As mentioned above in section 2.2.2, there are two competing schools of thought on how to overcome an air layer and effectively deliver coolant to the grinding zone. The velocity matching school, which is the conventional approach, claims that the velocity of the jet needs to be close to the surface velocity of the wheel. It should be noted that this approach is angle agnostic. The other school is that of Trmal and Kaliszer [18], who state that the angle modified jet momentum must exceed that of the air layer on the surface of the wheel.

These schools, and models built foundationally upon them, can be tested simply by directing jets of coolant at the surface of a wheel and recording what velocities result in wetting of the surface. To confirm that the visual inspection is accurate, two verifications were undertaken: a spindle power measurement and a wetting test that used a removable coating.

3.3.1 Visual Inspection

Two different sets of experiments were undertaken. The first was intended to compare the developed conditioner to the commercial nozzle, and to see what the differences were between them in terms of their ability to penetrate the air layer. In the second, a jet from the developed conditioner was directed at the wheel at various angles, to investigate the actual penetration requirements for a given momentum flux. Since the jet is coherent and has both a known area and a plug like velocity profile, an accurate and confident account of the interaction with the air layer and wheel surface can be

reported.

For the first test, the two jets were oriented horizontally to the work surface, and positioned 21 mm vertically and 270 mm horizontally from the lowest point of the wheel. The wheel was run at speeds ranging from 15.24 $^{m}/_{s}$ to 40.64 $^{m}/_{s}$ in 5.08 $^{m}/_{s}$ increments, and the velocity of the jet was brought above the hydraulic flip transition point, and then down to an appropriate velocity. To determine the critical velocity, the jet was brought to a "no contact" position relative to the wheel, and then a "full contact" position (based on Steffen's nomenclature, fig. 3.5). The volumetric flow rate was recorded at each position, and this process was repeated three times for each wheel speed. The critical flow rate was considered to be between the average "no contact" and "full contact" values.

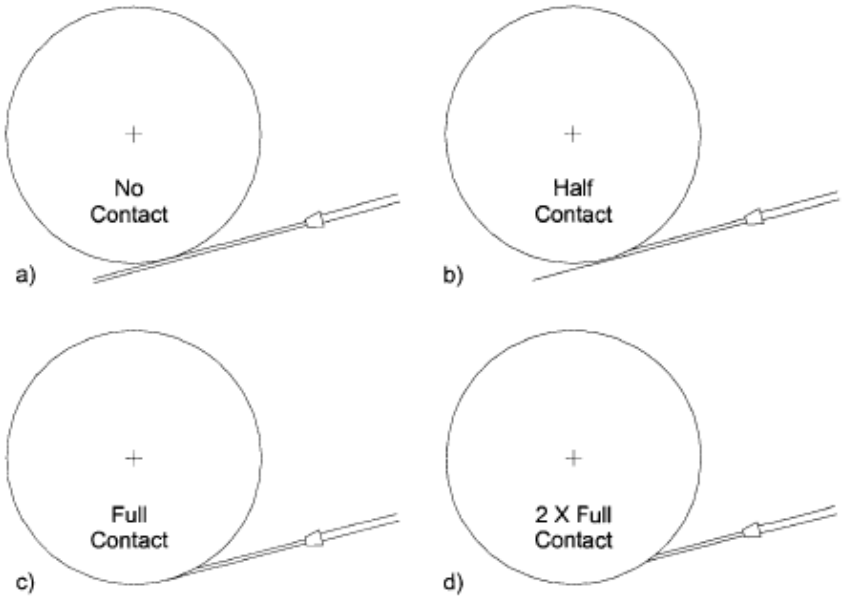

Figure 3.5: Description of jet-wheel contacts [45]

The second test concerned the impact of nozzle angle on the air layer penetration.

The nozzle was directed towards a point on the wheel periphery, 50 degrees ahead of the contact patch, at a consistent radial distance. The angle of the nozzle, relative to the tangent, was varied between 15 and 90 degrees in 15 degree increments, and the wheel between 10.16 $^{m}/_{s}$ and 40.64 $^{m}/_{s}$. A list of experimental conditions can be found below in table 3.2. A similar inspection to the above experiment was carried out, however in this case only "full contact" was sought.

Table 3.2: Experimental conditions for angled test

Characteristic	Range of Values
Wheel Speed (v_s)	10.16 $^{m}/_{s}$, 20.32 $^{m}/_{s}$, 30.48 $^{m}/_{s}$, 40.64 $^{m}/_{s}$
Nozzle angle (degrees)	15°, 30°, 45°, 60°, 75°, 90°
Radial distance	30 cm

3.3.2 Confirmation of Air Layer Penetration

It was deemed desirable to confirm that the jet of coolant was penetrating the boundary layer and wetting the surface of the wheel, rather than being diverted or redirected by the air layer.

A simple visual experiment was developed to see if the wheel surface was being wetted by the coolant jet, using a removable chalk coating. It was found that blue chalk provided the best contrast to the wheel surface, and showed the effect of the jet strikingly.

A more quantitative experiment was conducted by measuring the power consumption of the wheel as the jet was applied to it. When a jet hits a wheel moving at a higher surface velocity than the jet itself, the wheel acts like a pump and accelerates the fluid. The power required to accelerate the liquid is not negligible and can be both

predicted and measured. Gviniashvili [54] proposed an equation predicting the power requirement to accelerate a jet that hits a wheel at surface speed v_s, with volumetric flow rate $\dot{V}$, jet speed v_j, and jet density ρ.

$$P = \rho \dot{V} \left(v_s^2 - v_s v_j\right) \tag{3.4}$$

Adjusting this equation to account for the angle of impact relative to the wheel tangent α_t, which has an impact on the momentum contributed to the system by the jet in the direction of wheel rotation, provides equation 3.5.

$$P = \rho \dot{V} v_s \left(v_s - v_j \cos \alpha_t\right) \tag{3.5}$$

Irrespective of the mechanism of air layer penetration, the difference between the idling spindle power consumption and the power consumption when "loaded" with coolant is expected to be clear.

The wheel spindle is driven by a three phase motor, and the motor leads were passed through a Fast Response Universal Power Cell (UPC-FR) from Load Controls Inc. The UPC uses the Hall Effect to measure the power draw by measuring the magnetic field surrounding the power leads. The sensor has an output signal of zero to ten volts, which corresponds to a customizable range set by the user with a variable resistor. In this case, the resistor was set to 20.17 ohms, resulting in a full sensor range of 0-20.17 HP, or 15041 W. The signals were collected with a DATAQ DI-158-U, and recorded with DATAQ WinDaq software. The jet was applied with flow of 1.68 L/min, which corresponds to a velocity of 3.6 m/s. The wheel was run at 30 m/s, and the angle between the nozzle and the wheel tangent was varied between 0 and

90 degrees, in 15 degree steps. The spindle power consumption was measured and recorded in each position.

Based on modeling (expanded upon in section 4.2.1), the angle required to penetrate the air layer was predicted to be 28 degrees. The expectation is thus that there will be a stark power increase between 15 and 45 degrees, confirming the wetting of the wheel surface.

3.4 Relative Effective Flow Through Hydrodynamic Pressure

A simple method of comparing the efficacy of different nozzles at delivering cutting fluid to the grinding zone was desired. In section 2.1.2, the mechanism of transporting fluid through the grinding zone was discussed, and it is trivial to say that a more effective method of coolant delivery will allow more coolant into the grinding zone. Several researchers used force or hydrodynamic pressure measurements during grinding to quantify the effectiveness of fluid delivery techniques, and Ganesan et al showed that the normal force applied to a workpiece increased linearly with effectively delivered flow [87].

For this work, a simple method was developed to compare the efficacy of various nozzles at delivering coolant by using force measurements. A mild steel target was precision ground to a width of 4 mm, equivalent to the nozzle diameter. The target was attached to a Kistler MiniDyn 9256B dynamometer, and guards were placed in front of and beside the target (figure 3.6) to avoid side flow or jet spray from affecting the force measurements. The target was ground to a known height, and several spark-out passes (at zero depth of cut) were taken to ensure there was no spindle deflection. The nozzles were directed at the target surface, so that the resulting jet would be just above the target.

The jets were operated at two flow rates, 7.5 L/min ($\sim$15 $^{m}/_{s}$) and 15 L/min ($\sim$30 $^{m}/_{s}$), chosen to cover a range of values that would realistically be used in industry. Additionally, as these tests were conducted after the jet characterization tests whose results are reported in section 4.1.1, there was a desire to see how the differences in

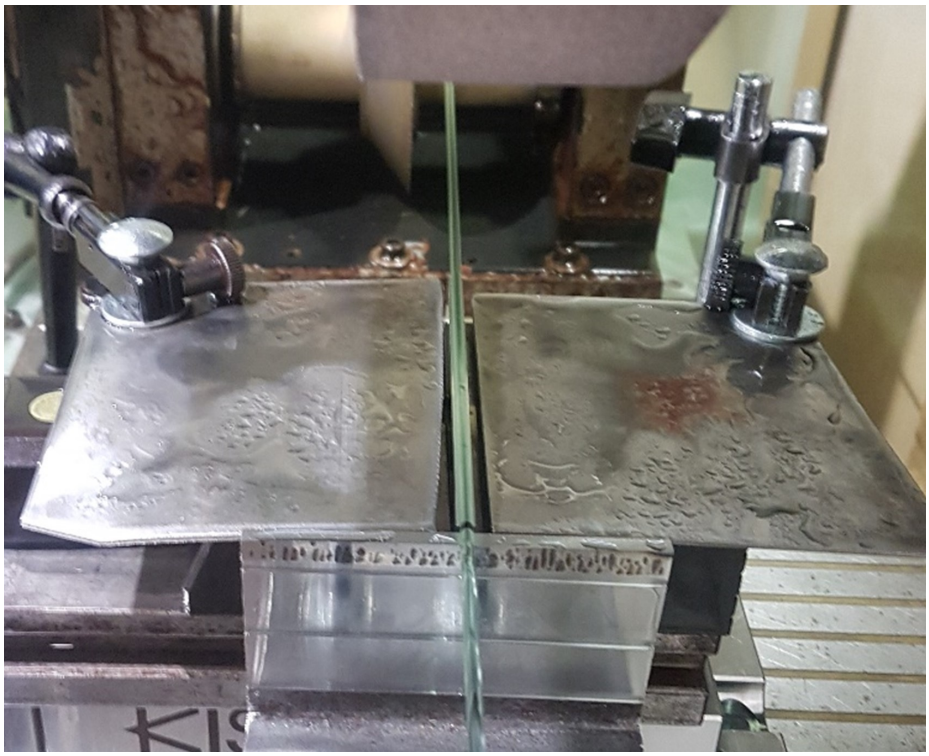

Figure 3.6: Jet positioned above target for hydrodynamic pressure test, with floating guards to prevent signal contamination from spray

jet divergence affected the measured pressure. The chosen flow rates are expected to clearly demonstrate any differences.

With the jet oriented above and parallel to the target surface, and operating at the test flow rate, the grinding wheel was run at 30 $^{m}/_{s}$ and lowered to a height of 25.4 µm (0.001 inches) above the target. The wheel was left in position for approximately 30 seconds, and then raised to a distant stand off. These tests were conducted for each nozzle and flow rate at distances of 30 cm, 45 cm, and 60 cm between the nozzle exit and the grinding zone.

The data was recorded and analysed with DynoWare, where built in tools were used to remove high frequency noise. Measurement drift proved to be a significant

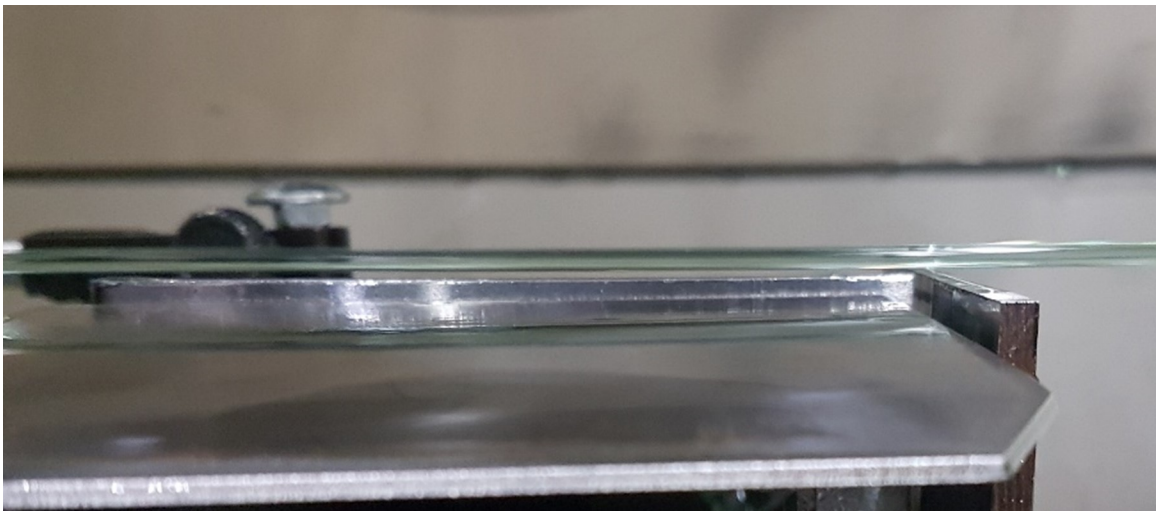

Figure 3.7: Coherent jet positioned above target for hydrodynamic pressure test

issue. To address this, the change in the signal as the wheel was brought down to position was recorded, as was the equivalent measurement when the wheel was being lifted. These two values show the near instantaneous difference between a free condition and a condition where the interaction between the wheel, the fluid, and the target workpiece is generating a hydrodynamic pressure.

3.5 Critical Material Removal Rate and Burn Tests

Operators who use grinding processes are concerned with surface quality and the productivity of their work. A burn test can be considered the final say in an investigation of the effectiveness of coolant delivery methods because it clearly shows and contrasts the limits of productivity before catastrophic reductions in surface quality occur. Covered in depth in section 2.1.3, grinding burn occurs when the grinding heat flux overwhelms the ability of the coolant to remove it, leading to a transition from nucleate boiling to film boiling, and a rapid rise in temperature in the grinding zone. Steffen showed that this transition is marked by a dramatic increase in spindle power, shown in fig. 2.5, also known as the "surge" [45].

During a burn test, a workpiece is ground at increasing depths of cut, and is observed to determine the onset of burn. While certain previous works have used sloped workpieces to allow for a continuous range of depths of cut, in this work it was deemed more accurate to use a flat workpiece and to take repeated trials at discrete depths of cut.

In these tests, a precision ground 4 mm wide workpiece was oriented parallel to the path of the grinding wheel. The use of a dial indicator ensured that the wheel and workpiece were in line with one another. The jet was set to the working flow rate, and directed parallel to the workpiece, positioned just slightly above the surface.

Before each trial, the wheel was jogged slightly in the axial direction. This was done to avoid contamination between tests, such as wheel glazing due to burn or wheel collapse. The workpiece was then ground down to ensure an initial cutting depth of zero, and the orientation of the jet relative to the workpiece was confirmed before the test was begun.

In each test, the workpiece was ground in increasing depths of cut, incrementing each time by 12.7 µm. At each depth of cut, the workpiece was ground in an up-grinding pass, followed by a down-grinding pass after the wheel was lowered the same amount. After the down-grinding pass, the wheel was lowered to the next depth of cut setpoint and the process continued. The spindle power was recorded using the UPC from Load-Controls Inc, described in section 3.3.2.

The grinding wheel was operated at a consistent 30 $^{m}/_{s}$, and the workpiece was fed at a rate of 20 $^{mm}/_{s}$. Flow rates of 7.5 L/min and 15 L/min were utilized, similar to the force tests, and stand-off distances were varied between 30 cm and 45 cm. A full list of experimental conditions are listed in table 3.3.

Table 3.3: Experimental conditions for grinding burn tests

Characteristic	Range of Values
Wheel Speed (v_s)	30 $^{m}/_{s}$
Feed Rate (v_w)	20 $^{mm}/_{s}$
Jet Flow Rate ($\dot{V}$)	7.5 L/min, 15 L/min
Jet Stand-offs	30 cm, 45 cm
Depths of Cut (a_e)	0 µm - 127[3]µm

The experiment was run at increasing depths of cut, and observations such as sparking and workpiece discolouration were noted. When significant burn occurred, which was determined both by observing the grinding process and through dramatic changes in the spindle power, the trial was ended. An example power trace for this experiment can be seen in fig. 3.8.

The expectation is that there will be a gradual increase in consumed power with increasing depths of cut, followed by a dramatic increase as grinding burn commences.

[3]127 µm was the maximum depth of cut achieved in the test, but most trials did not reach that depth. Each trial was ended after the occurence of significant burn, to protect the apparatus.

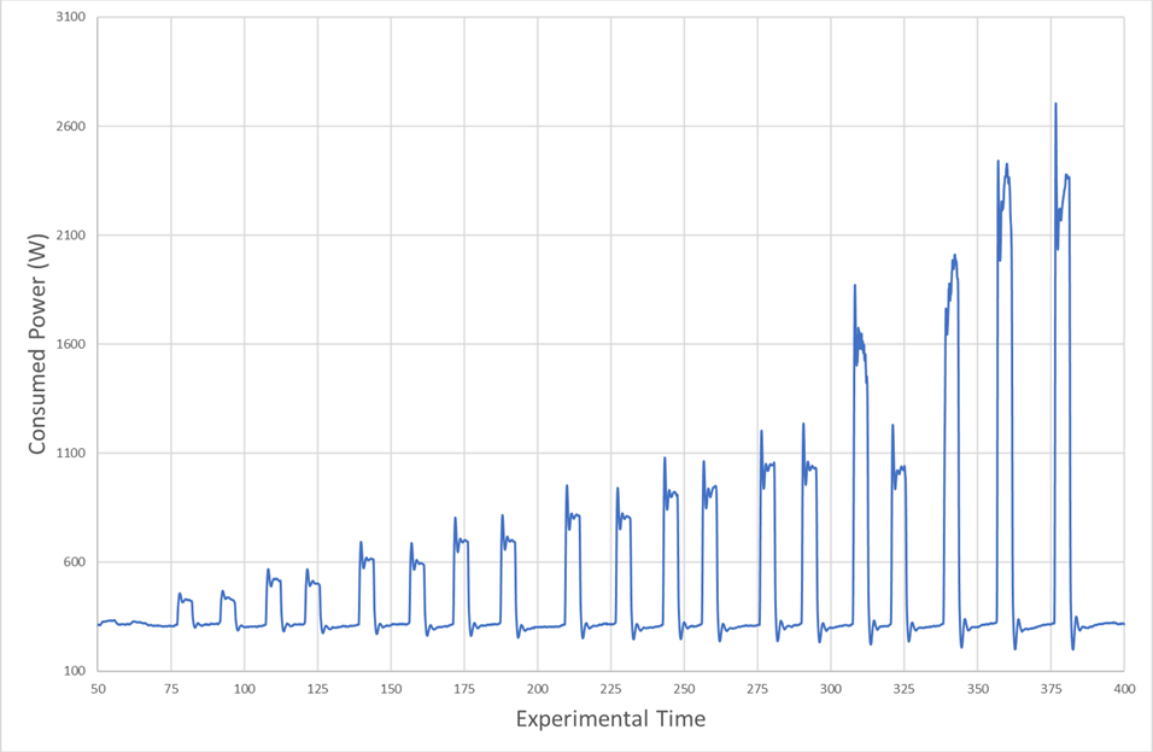

Figure 3.8: Example power trace in burn trial (developed conditioner, $\dot{V}$ =15 L/min, 30 cm stand-off)

The developed conditioner is expected to delay the onset of burn compared to the Rouse nozzle, and higher flow rates and shorter stand-off distances are expected to outperform lower flow rates and higher stand-off distances.

Chapter 4

Results and Discussion

The developed conditioner was characterised and compared to the Rouse nozzle, often considered the best commercially available nozzle for coherent jets. Structural characteristics were investigated, both qualitatively and quantitatively through visual and direct measurements, and the flow separation and reattachment characteristics were determined. A model to predict the conditions required to penetrate the air layer was developed and tested, with experimental results agreeing closely with predictions. Two different tests of cooling ability were carried out, the first to determine the relative effective flow rates between cases, and the second a burn test to show the ultimate effectiveness of the cooling jets on a grinding operation.

4.1 Jet Structural Characteristics

The structural characteristics of the jets are compared in three different ways. The first section, *Dispersion*, visually compares the structure of the jets and the coherence at different points and velocities. Each jet begins with a contiguous structure, which gradually changes as the jet interacts with the surrounding atmosphere. This interaction is self reinforcing, as small surface waves will be amplified and result in eventual ligament and droplet breakoffs. A jet that is initially laminar, without surface perturbations, will resist breakup for greater distances and flow rates than a turbulent jet.

The second section, *Hydraulic Flip*, focuses on the impact of flow separation that increases jet coherence and decreases jet diameter when a critical velocity is reached. Determining when this separation occurs, and the point at which it is erased, is vital to using both the Rouse nozzle and the present work.

The final section, *Momentum Fluxes*, investigates the internal structure of the jets as they impact surface. Based on the profiles of the measured impact force, the extents of the jet and the dispersion can be determined and compared confidently. These structures will definitively show how coherent each jet is.

The diameter of the jets issuing from both the developed conditioner and the Rouse nozzle were measured with high speed camera images, and were found to have diameters of 3.2 mm after hydraulic flip. Unless otherwise noted, all velocities in these results are based on this separated diameter, and not the nozzle diameter.

4.1.1 Dispersion

High speed images of the jets at various velocities and stand-off distances show a clear difference with regards to the onset of jet breakup and the coherence lengths.

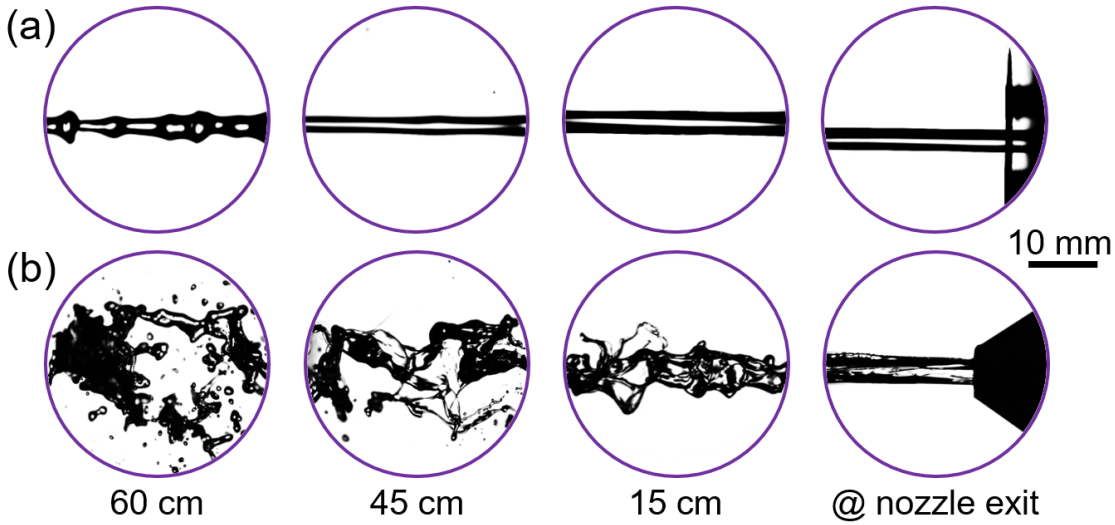

Figure 4.1: Jet structure for developed conditioner (a) and Rouse nozzle (b) at 20 $^{m}/_{s}$

Figure 4.1 compares the Rouse nozzle and developed conditioner at stand-off distances of up to 60 cm for a jet velocity of 20 $^{m}/_{s}$. The Rouse nozzle shows striations on the jet surface immediately after leaving the nozzle, with jet breakup starting as soon as 15 cm away. Breakup increases dramatically by 45 cm, and the jet appears to be entirely aerosolized 60 cm away from the nozzle exit. By contrast, the jet issuing from the developed conditioner appears completely smooth, with no striations or perturbations as it leaves the nozzle. The jet remains coherent at 15 and 45 cm, generating only the slightest of surface irregularities until 60 cm, where some axisymmetric surface waves and instabilities can be seen. Critically, the jet from the developed conditioner at 60 cm appears more laminar and coherent than the jet issuing from

the Rouse nozzle at 0 cm.

Complementing figure 4.1, figure 4.2 compares the two nozzles by presenting jets ranging from 10 m/s to 50 m/s at a stand-off distance of 30 cm.

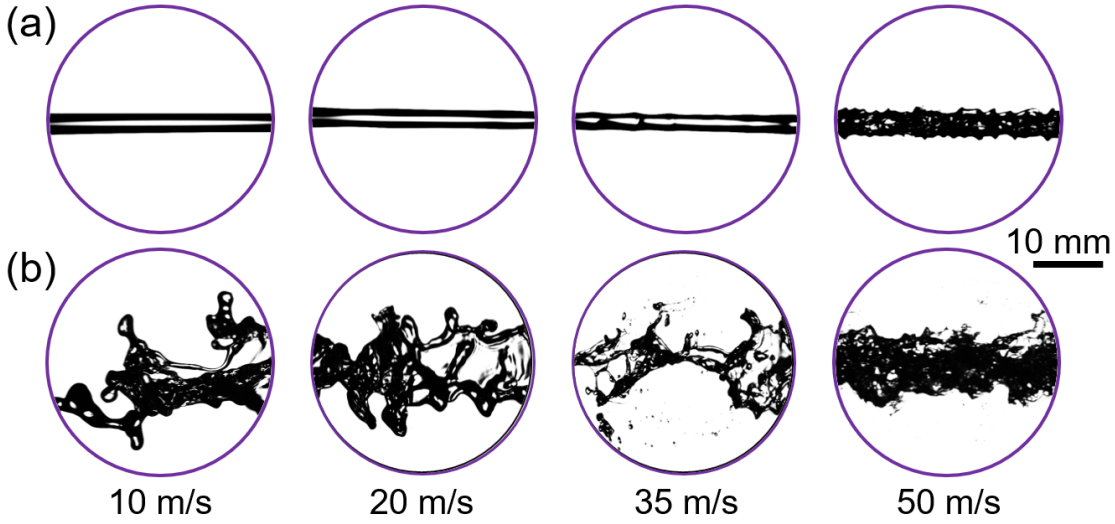

Figure 4.2: Jet structure for developed conditioner (a) and Rouse nozzle (b) at 30 cm from the nozzle exit

For the jet issuing from the developed conditioner, surface waves do not appear until a velocity of 35 m/s, and while significant ligaments are in evidence at 50 m/s, the jet can be seen to maintain its bulk structure. Jets from the Rouse nozzle begin to break up at velocities as low as 10 m/s, and this trend continues with increasing velocities. By 35 m/s the jet core appears compromised, and the jet is essentially an aerosolized plume.

Apart from the 50 m/s case in figure 4.2a, the jet issuing from the developed conditioner is coherent in every image. Conversely, the Rouse nozzle provides a coherent jet only at that the nozzle exit in figure 4.1b, as the jets quickly diverge to over twice their initial diameter with large surface waves that entrain air. While

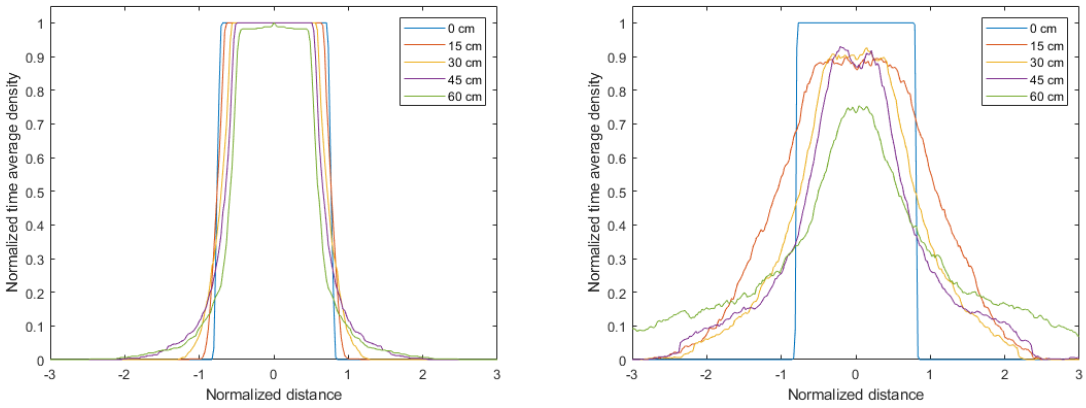

(a) Developed conditioner (b) Rouse Nozzle

Figure 4.3: Time averaged density profiles of the jets at 20 $^{m}/_{s}$, plotted over normalized distance with respect to the nozzle diameter

these high speed images provide just snapshots from a single moment in time, a time averaged perspective can be obtained by analyzing the extents of the jets. Above, in figures 4.3a and 4.3b, the time averaged jet densities of the two jets at various stand off distances are contrasted.

Under these conditions, the difference in jet breakup is clear. Both jets begin with plug-like flows at the nozzle exit, but only the developed conditioner maintains it over any distance. In fact, the profile of the developed conditioner barely changes, even to the maximum stand-off distance of 60 cm. The jets from the Rouse nozzle, by contrast, quickly degenerate into a lower, wider distribution, illustrating the divergence over distance.

The jet coherency for each stand off distance is shown in figure 4.4. The test for coherence that was defined in section 3.2, based in turn on Webster's criteria, is that a jet ceases to be coherent when its diameter reaches twice that of the nozzle. Based on that test, the jets from the Rouse nozzle lose coherence before 15 cm. For the

Figure 4.4: Comparison of jet coherency (20 m/s jets)

developed conditioner, the coherence never exceeds 1.6.

Using the same time averaged density method, the jets at a range of velocities (shown in figure 4.2) are analyzed. For the developed conditioner (figure 4.5a) there is very little change in dispersion at speeds below 40 m/s, with the profiles essentially overlaying one another, and a dramatic change only occurring at 50 m/s. Even then, the measured profile is fairly rectangular. This suggests that the jet is maintaining its core, but is also subject to growing surface waves. These waves are slowed by the surrounding air, and so grow the extents of the jet without reducing the time averaged density. This reveals the limitation of this visual inspection, as it can not describe the structure of the jet interior.

Figure 4.5b shows the contrast with the jets issuing from the Rouse nozzle. Even at the lowest flow rate, the jet has lost the sharp edges and constant diameter of a coherent jet. As the jet velocity increases, the observed dispersion increases, to the point where the diameter of the 50 m/s jet approaches four times that of the nozzle.

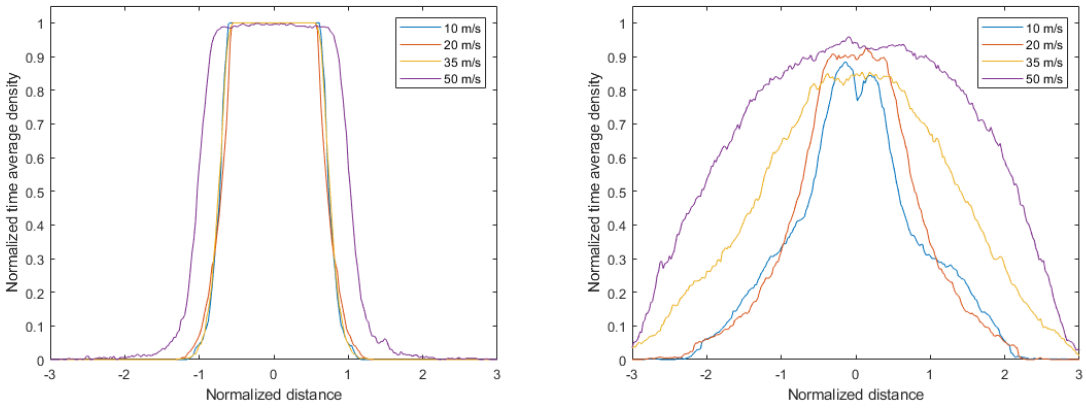

(a) Developed conditioner (b) Rouse nozzle

Figure 4.5: Time averaged density profiles of the jets at 30 cm, plotted over normalized distance with respect to the nozzle diameter

4.1.2 Hydraulic Flip

An important component of jet characterization is characterising the hydraulic flip. At low flow rates the flow separates from, and then reattaches to the nozzle wall due to the contraction, and leaves the nozzle disturbed. At the critical flow rate, the flow transitions to be cleanly separated from the nozzle, with no reattachment. This is called hydraulic flip.

The phenomenon is shown in figure 4.6, which tracks the transition in four steps, each 1/500 of a second apart. Figure 4.6a shows a diffuse aerosolized flow, figures 4.6b and 4.6c show the beginning and end of the transition, and figure 4.6d shows the onset of the laminar flow. It must be noted that hydraulic flip will not always result in laminar flow as it only eliminates nozzle effects, not upstream turbulence.

Separation occurs once the flow rate reaches a critical value, but this value differs between nozzles. Researchers [77, 79] have described the existence of a hysteresis effect, where the flipped characteristics of a jet may be maintained below the critical flow rate to another, lower velocity, and only then will the flow reattach to the nozzle. Knowing these points is instrumental to characterizing the jet and the nozzle for the various experiments conducted. Using the imaging techniques used in the dispersion analysis, the critical flow rates were determined.

In the case of the developed conditioner, hydraulic flip occurs around 9 L/min (approximately 12 $^{m}/_{s}$, nominal velocity) and the flipped jet persists until the flow rate is reduced to below 1 L/min (1.5 $^{m}/_{s}$, nominally). The Rouse nozzle requires a significantly higher flow rate to separate from the nozzle wall, with hydraulic flip occurring only around 14 L/min (18.5 $^{m}/_{s}$), and then persisting until the flow rate is between 7 and 5 L/min (8 $^{m}/_{s}$).

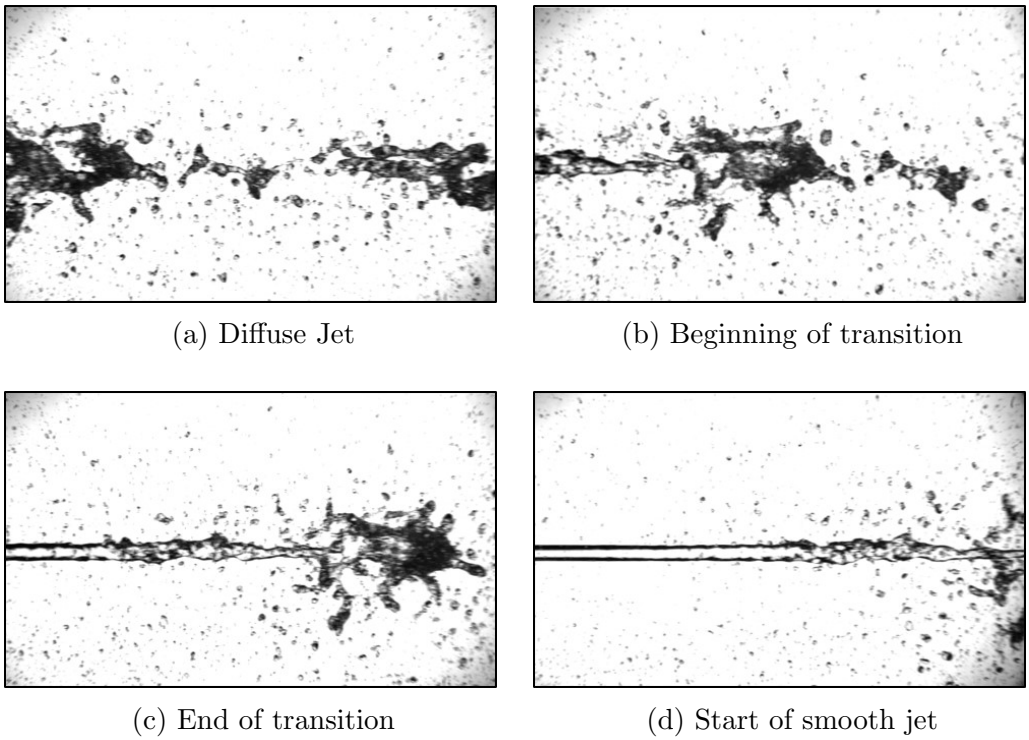

(a) Diffuse Jet (b) Beginning of transition

(c) End of transition (d) Start of smooth jet

Figure 4.6: Transition of a jet through hydraulic flip. Jet is moving left to right at approximately 9 L/min.

The low critical points in the developed conditioner provide much greater utility to an operator, allowing them to generate a highly coherent jet even at very low velocities. This flexibility would cover nearly any conceivable use case, from higher flow rates in high speed grinding to precision coolant delivery in drill cutting and honing. The Rouse nozzle both requires a higher flow rate to achieve hydraulic flip, and loses those characteristics at flow rates five times higher than the developed conditioner.

4.1.3 Momentum Fluxes

The final component of characterizing the developed jets is the result of the momentum flux measurements. Through this experiment, an analog to the velocity profile may be generated, and compared between different nozzles and stand-offs. Jets issuing from the developed conditioner and the Rouse nozzle were characterized at a velocity of 15 $^{m}/_{s}$.

The measured forces for the experiments are plotted below, in figure 4.3. A coherent jet will have a narrower force profile than a diffuse jet, and that profile will persist over further distances from the nozzle. Theoretically, a perfect jet measured as it leaves the nozzle, without any time to expand or disperse, would have a maximum force reaching the value calculated by equation 4.1, where ρ is the liquid density, A_j is the jet area, and v_j is the jet velocity.

$$F = \rho A_j v_j^2 \tag{4.1}$$

The above equation provides a theoretical maximum of 1.8 N for a 3.2 mm jet with a speed of 15 $^{m}/_{s}$. Even though a coherent jet would maintain a consistent radius, the width of the target (4 mm) must be accounted for. As a result, the measured force would appear between -2 and +2 radii, along the horizontal axis. A less coherent jet will have a lower maximum measured force and will have a larger spread, and both of those characteristics would be expected to intensify with an increasing stand-off distance.

The results of this experiment clearly show the differences in jet coherence and the impact – or lack thereof – of the stand-off distance on dispersion. The force profile

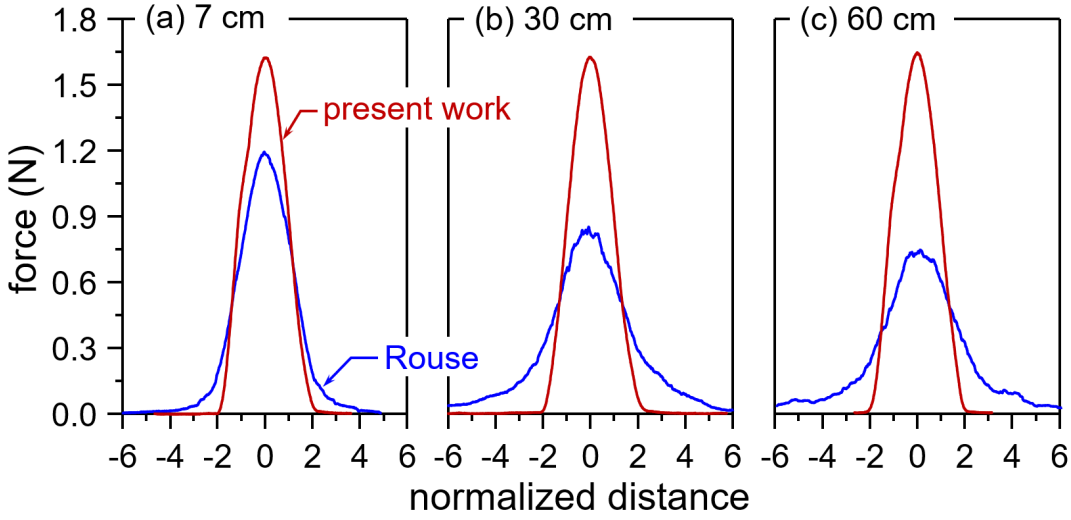

Figure 4.7: Force traces for the developed conditioner (present work) and Rouse nozzle at various stand-offs, for a jet flow rate of 7.5 L/min

of the jet issuing from the developed conditioner is tall and narrow. The extents are within the ± 2 radius boundary that is expected for an entirely coherent jet, and the sharp transitions at that boundary show that the jet edge cleanly separates from the target as it passes. The peak force measured approaches the calculated value, showing that the jet maintains and delivers its momentum with minimal losses. Critically, these characteristics are maintained across all stand-off distances, to the extent that it would not be possible to predict the nozzle stand-off of each case by inspection of the force trace alone. The jet does not spread, deform, or break up over increasing distances, which is the qualitative definition of a coherent jet.

The extents of the force traces for the Rouse nozzle are much wider and do not remain consistent with distance. The transitions at the trace edges are gradual rather than sharp, suggesting break up on the jet surface. The overall shape of each trace is lower and wider than those of the developed conditioner, and appear to resemble a

gaussian distribution, which would occur in diffuse jets. The peak measured force is considerably lower than the expected force for this flow rate and initial jet area, and decreases with increasing nozzle stand-off, showing that the breakup of this jet is not confined to waves on the surface, but also extends to the core. These results depict a jet that quickly loses coherence.

It should be noted that despite the quick decay, the influence of hydraulic flip can be seen in these results as well. An unseparated jet with a flow of 7.5 L/min would have, from equation 4.1, a maximum force of 1.16 N. Even though it is already somewhat diffused and dispersed, the Rouse nozzle at 7 cm has a maximum measured force of 1.2 N. This both confirms the influence of hydraulic flip in this case, and the idea that hydraulic flip alone is not sufficient to generate a coherent jet, without consideration of upstream conditions.

4.2 Penetration of Air Layer

Investigations into the penetration of the air layer began with a consideration of the underlying physics and the development of a model to predict the critical jet speed for air layer penetration. Experiments on jet penetration were completed, and the model was validated against these results, showing a strong correlation between predicted and real-world values. Finally, the visual tests showing wetting of the wheel surface were confirmed through direct measurements. The results here show that the air layer can be pierced, and the wheel surface wetted, by jets with velocities below 25% that of the wheel surface.

4.2.1 Air Layer and Jet Modeling

As described at length in section 2.2.1, there are two main schools of thought regarding the penetration of the air layer around the rotating wheel by a coolant jet. The conventional opinion is that the speed of the jet must be equal to the surface speed of the wheel in order to overcome the boundary later [8]. Trmal and Kaliszer brought forward the idea that the momentum of the air layer has to be overcome by the jet - specifically the component of the jet momentum that "flows up" the wheel upon impact. Unfortunately, neither Trmal and Kaliszer nor subsequent researchers who use this method [18, 52] propose a way of predicting the velocity profile of the air layer but instead use in-situ measurements in their work. This is an inconvenient solution in industrial production settings, and as it would be beneficial for industry and research to have a predictive tool a model was developed to fill this gap.

Equation 2.8, repeated here as equation 4.2, uses the height and average velocity of the air layer to calculate the momentum flux per unit width, both of which are less

than precise values.

$$M_{\text{air}} = \rho \cdot h_{\text{air}} \cdot \bar{u}_{\text{air}}^2 \tag{4.2}$$

In place of the thickness of the air layer, the momentum thickness of the boundary layer is used. Momentum thickness can be calculated with equation 4.3, where t is the distance away from the surface, $u(t)$ is the fluid velocity as a function of the height, and v is the free stream velocity [74].

$$\Theta = \int_0^\infty \frac{u\,(t)}{v}\left(1 - \frac{u\,(t)}{v}\right) dt \tag{4.3}$$

In this case, the free stream velocity can be considered to be the wheel peripheral speed v_s. Equation 4.2 then becomes

$$M_{air} = \rho \cdot \Theta \cdot {v_s}^2 \tag{4.4}$$

Equation 4.3 requires the velocity profile $u(t)$ as an input, of which two exist in the literature. Radhakrishnan's relation (equation 2.9) considers both the wheel speed and the surface roughness. However, this prediction does not tend to zero at large distances away from the wheel surface. This would result in an infinite momentum thickness, which is not realistic. Alenius and Johansson's correlation (equation 2.11) is solely a function of the wheel speed, and does converge to zero. Since the relation is a dimensionless velocity profile, the momentum thickness is rendered constant at approximately 2.4 mm. Due to the limited experimental conditions used to develop this empirical relation, there is a concern that the profiles may not be generalizable to all cases.

The thickness of a turbulent boundary layer over a smooth, flat surface is often

approximated by the one-seventh power law profile [74], where the Reynolds number is a function of the air density and viscosity, the surface speed v_s, and the distance along the flat surface x.

$$\Theta = x \cdot \frac{0.016}{Re_x^{1/7}} \tag{4.5}$$

$$M_j = \rho_j \cdot d_j \cdot v_j^2 \tag{4.6}$$

$$M_j' = M_j \frac{1 - \sin \alpha_n}{2} \tag{4.7}$$

Here the characteristic length is taken to be the distance along the circumference of the wheel from the point of contact with the work surface to the point of impact of the jet.

A program was written in MATLAB to predict the jet velocity required to penetrate the air layer. Starting with the nozzle position [including the angle relative to the horizontal and the vertical and horizontal distances from the wheel-workpiece contact point] and an initial jet velocity of 5 m/s, the trajectory of the jet is tracked until it reaches the wheel surface, where the impact angle and point of impact are determined. The modified jet momentum is calculated using the impact angle and compared to the momentum of the air layer. An iterative approach is used, increasing or decreasing the jet velocity based on the relative values of the air and modified jet momentum. The process continues until those values are within a window of 0.05 kg/s^2 of each other.

4.2.2 Visual Inspection of Air Layer Penetration

Through visual inspection, critical flow rates to penetrate the air layer were determined for the two nozzles. These are recorded in figure 4.8, along with the nominal jet speed based on the nozzle area. These results appear to confirm the two-fold hypothesis of this work, which is that (a) the air layer can be penetrated with a jet moving at a fraction of the wheel speed and (b) that a coherent jet will more readily penetrate the air layer than a diffuse jet.

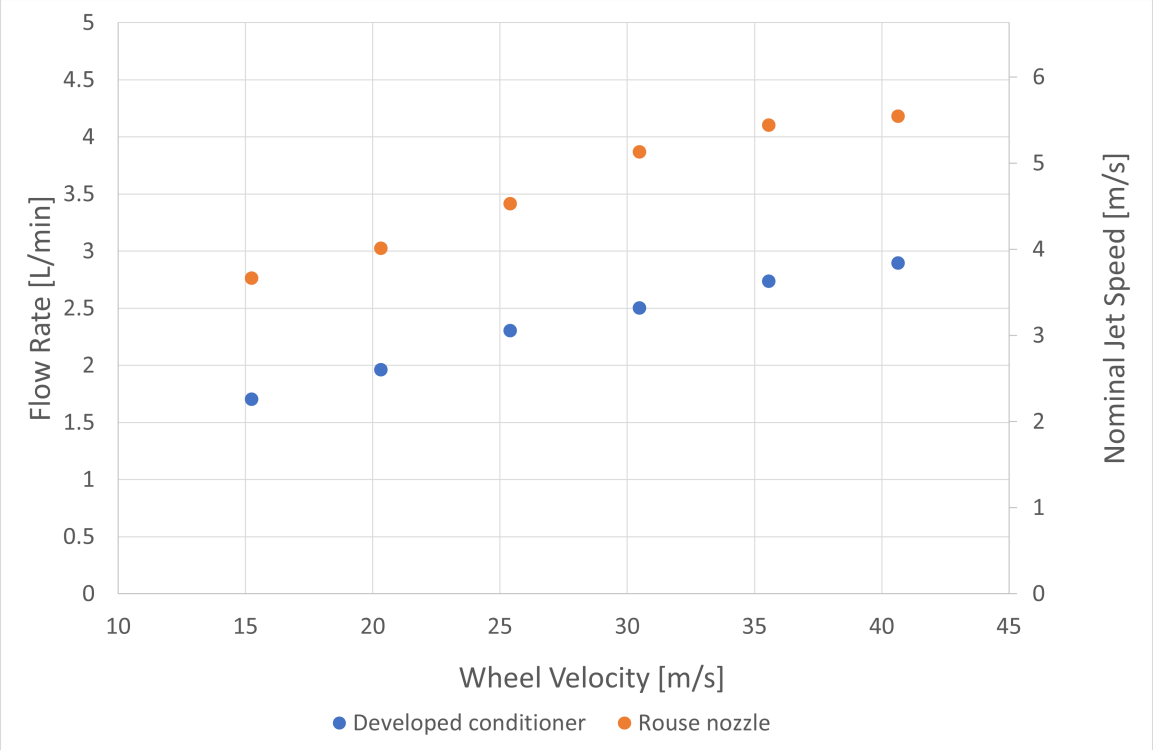

Figure 4.8: Critical flow rates required to penetrate the air layer, based on visual inspection (27 cm stand off)

However, the effect of the hydraulic flip must be accounted for. The extent of the hysteresis was investigated in section 4.1.2, and it was determined that while the effects persist in the developed conditioner to flow rates below 2 L/min, those same

effects for the Rouse nozzle are erased around 6 L/min. Consequently, the jet issuing from the developed conditioner should be analyzed with the reduced diameter of 3.2 mm, and the Rouse nozzle with the nozzle diameter of 4 mm.

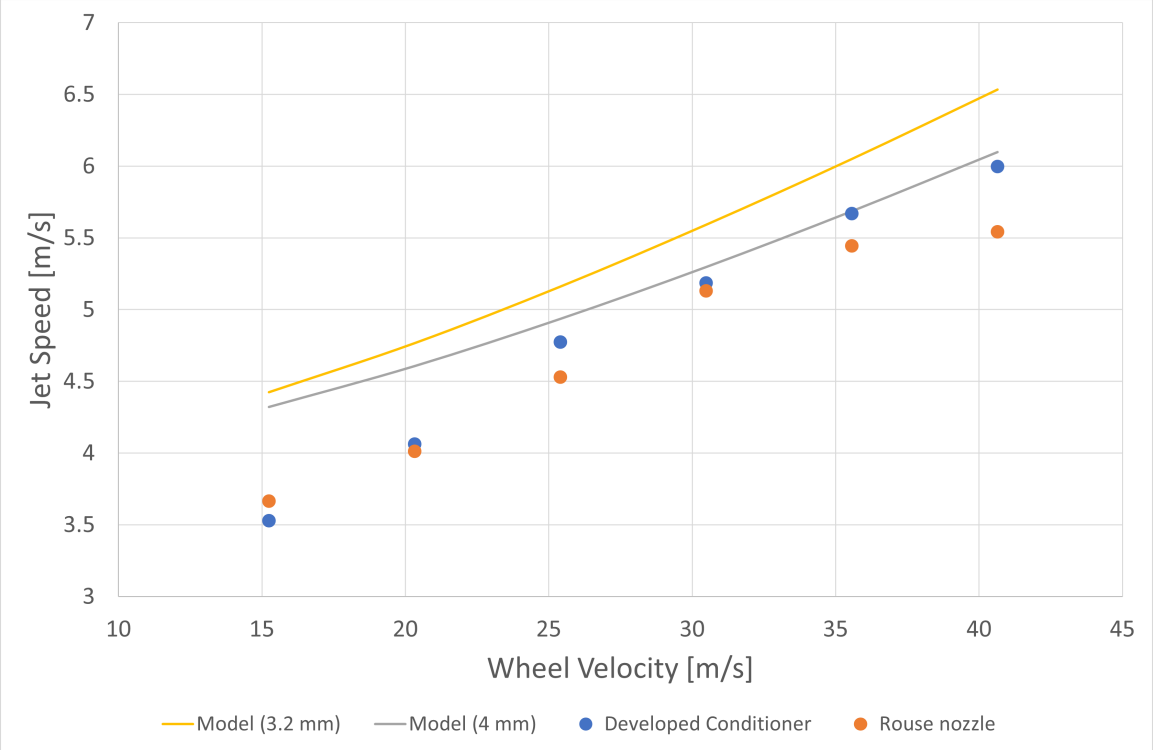

Figure 4.9: Critical jet speeds to penetrate the air layer, based on visual inspection (27 cm stand off)

Accounting for these actual jet diameters in figure 4.9 we can see that the velocities required to penetrate the air layer are essentially identical between the developed conditioner and the Rouse nozzle. These velocities are, however, an order of magnitude below the wheel velocity. Figure 4.9 shows that the model predictions are close to experimental values and experimental trends, with a slight over prediction of the required jet velocity.

The second part of this experiment was to investigate the impact that nozzle angle

had on air layer penetration. From Trmal and Kaliszer's work, and Akiyama et al's experimentation [14, 18], it is expected that a jet oriented normal to the wheel would more readily penetrate the air layer.

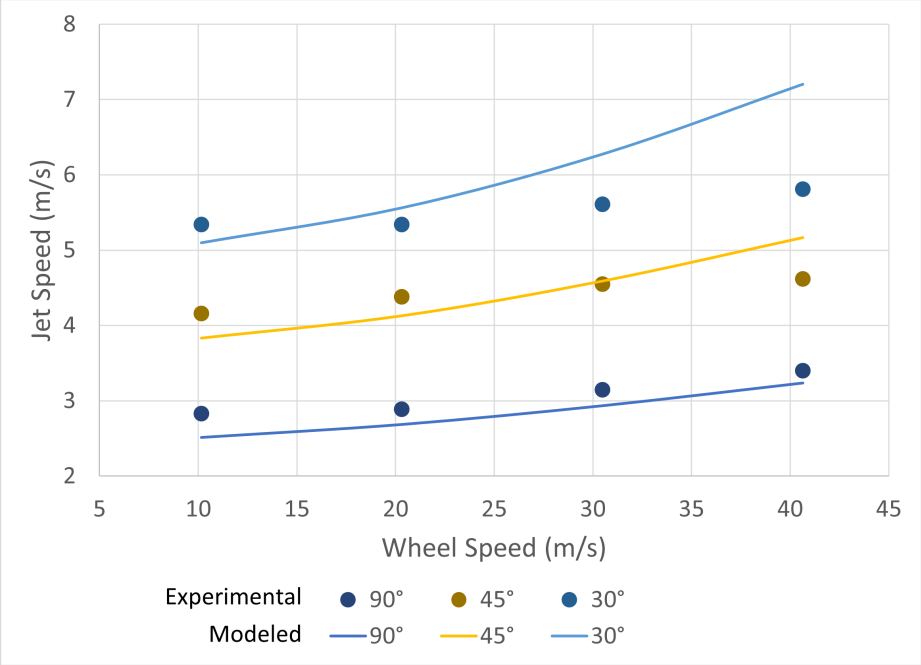

Figure 4.10: Experimental and modeled critical velocities to penetrate the air layer at different nozzle orientations

The results in figure 4.10 align with these expectations. Critical velocities required to penetrate the air layer and wet the surface of the grinding wheel are a function of the nozzle angle, with nozzles oriented normal to the wheel requiring a lower velocity to wet the wheel surface than those oriented closer to the tangent. Comparison with the model is also seen in figure 4.10, where the influence of the jet impact angle on the jet momentum (the $\frac{1-\sin\alpha_n}{2}$ term) appears to provide a fairly good representation of critical velocities, particularly at lower wheel speeds. The model appears to over predict the influence of the impact angle, however, at higher wheel speeds. Overall,

this analysis demonstrates the impact that nozzle angle and wheel speed have on the critical jet speed required to penetrate the air layer. Counter to the conventional knowledge, it is most effective to orient the nozzle normal to the wheel rather than tangentially, to most effectively wet the wheel. It is also clear that matching the momentum of the air layer with the jet is a more precise method of penetrating the air layer than matching the wheel surface velocity.

4.2.3 Confirmation of Air Layer Penetration

Two experiments were carried out to confirm the visual inspection method of whether the jet wetted the surface of the grinding wheel; one where a removable powder was applied to the surface, and one where the spindle power was recorded as the nozzle angle was varied. Both experiments confirmed that the liquid jets were, rather than being deflected by the air layer, penetrating it and wetting the surface of the wheel. In the first experiment, chalk was applied to a wheel and expected to be washed off by the impact of the jet. This can be clearly seen in Figure 4.11, where 4.11a shows the wheel with the chalk intact, and 4.11b shows the path cleaned by the jet as it hits the wheel surface.

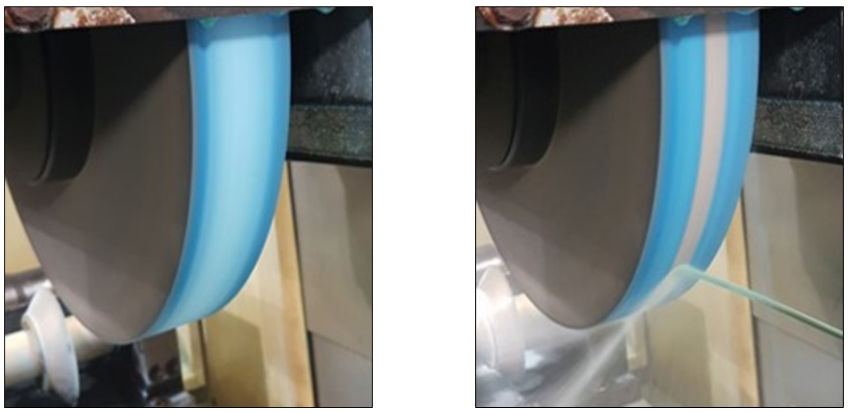

(a) Before contact with jet (b) After contact with jet

Figure 4.11: Grinding wheel operating at 30 $^{m}/_{s}$ with removable blue coating, interacting with 15 $^{m}/_{s}$ jet at 30 cm stand-off

The second experiment focused on the power consumption of the wheel as a liquid jet was introduced to it. The expectation was that the 3.6 $^{m}/_{s}$ jet would not penetrate the air layer at low contact angles (below 28°, based on the momentum model) and, at higher angles, the spindle power would increase, indicative of jet penetration and contact with the wheel periphery.

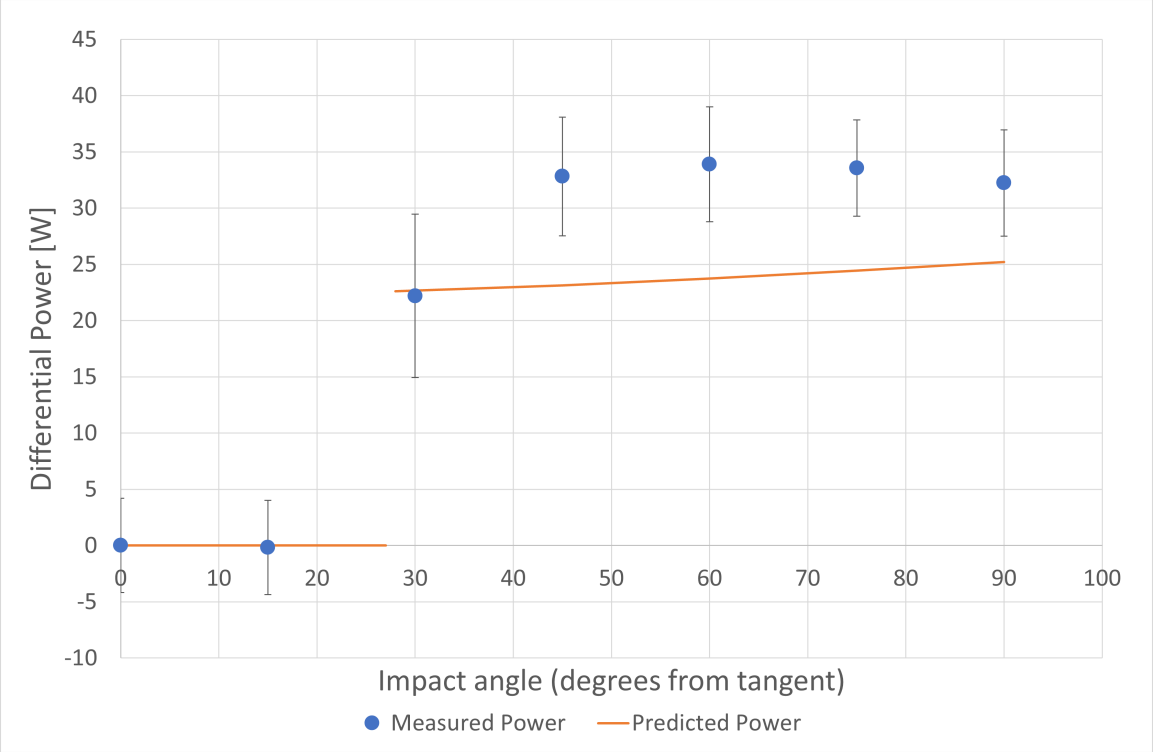

Figure 4.12: Power consumption of a grinding wheel impacted by a coolant jet

This is exactly what was observed. In figure 4.12 the differential power consumption remained steady at zero watts (relative to running at 30 $^{m}/_{s}$ with no jet) for both 0° and 15°, increasing to 22.4 W at 30°, then around 32 W for higher angles up to 90°. This agrees with the prediction, calculated with equation 3.5 from the jet and wheel velocity, fluid density, and contact angle, of 22.6 W at 30°.

The results of these two experiments are to confirm the visual inspection and the overall penetration of the air layer, with confidence.

4.3 Relative Effective Flow through Hydrodynamic Pressure

The relative effective flow experiments were conducted to determine which delivery conditions were most effective at delivering coolant to the grinding contact zone. Cooling effectiveness is highest when the grinding zone and the wheel-workpiece interface are saturated with liquid coolant. The lack of coolant, or the presence of a two-phase coolant and air mixture, will result in poor heat transfer.

Those same conditions will have an impact on the hydrodynamic pressure, where higher effective flow rates will result in higher hydrodynamic pressures. A 400 mm diameter wheel of type A60K8V was rotated at 30 $^{m}/_{s}$, 1 thousandth of an inch above a 4 mm wide target. The full experimental procedure is described in section 3.4. The differential forces were measured as the wheel approached and was removed from the target, ensuring that other system influences have no impact on measurements.

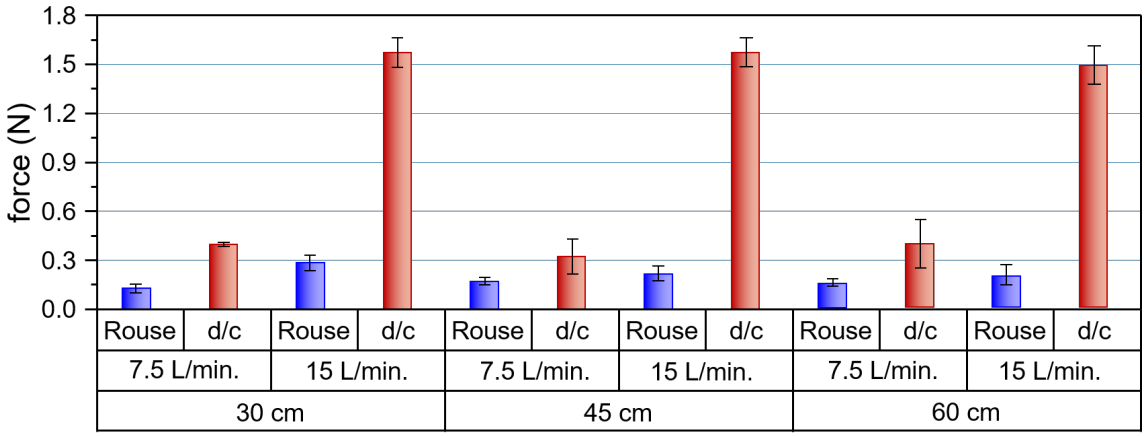

Figure 4.13: Normal force due to generated hydrodynamic pressure

In every trial of a common stand off distance and flow rate, the developed conditioner had a higher normal force than out performed the Rouse nozzle in terms of transmitted force. Stand-off distance does not appear to have a significant effect on the transmitted force. The recorded values were consistent across the entire range of stand off distances for all the developed conditioner trials, and for the Rouse nozzle's 7.5 L/min trial. This conforms with expectations for the developed conditioner, which the jet characterization from previous sections shows has a consistently coherent jet under these test conditions. Minor surface waves may start to form, but the bulk structure of the jet remains together.

In the 15 L/min case, the force measured for the Rouse nozzle decreased as stand-off distance increased. In figure 4.3, one can see that while the Rouse nozzle generates a diffuse jet, the dispersion increases only slightly between 30 cm and 60 cm, for a 7.5 L/min flow. The higher speed of the 15 L/min jet increases the dispersive impact, which manifests as a decrease in measured force as the stand-off distance increases.

While trends are important, it is also valuable to investigate how the measured values compare to each other in the test. The average values for each nozzle and flow rate are shown below in table 4.1. Stated previously in section 3.4, the applied force due to hydrodynamic pressure is linearly related to the effective flow rate. Assuming that the nozzles have broadly the same effectiveness of delivery between flow rates, it is expected that the measured pressure would double with the increase in flow, but the results do not reflect this expectation.

Table 4.1: Average force values for each flow rate, for each nozzle

	7.5 L/min	15 L/min	Ratio
Rouse nozzle	0.15 N	0.23 N	1:1.5
Developed conditioner	0.37 N	1.5 N	1:4.2

Table 4.1 shows that the Rouse nozzle generates a force around one and a half times higher in the 15 L/min case than in the 7.5 L/min case. By contrast, the change between those cases for the jet generated by the developed conditioner is greater than a four fold increase.

This points to the influence of factors beyond the volume of fluid supplied by the nozzle, such as the increased dynamic pressure generated when the jet strikes a surface. Per equation 4.1, the pressure scales exponentially with v_j, and would be helping to push fluid into the grinding contact. That the flow rate of 15 L/min is approaching the 4 L/min·mm value suggested by previous studies, and that the jet is matching the wheel velocity, are worth considering.

The increase in dispersion of the jet issuing from the Rouse nozzle - due to the higher velocity - may offset these supplementing conditions, resulting in a low increase in applied force. The jet issuing from the developed conditioner maintains coherence at the higher velocity, and can effectively and precicely deliver the coolant to the grinding zone. The effective delivery of the coolant, combined with the velocity matching and the suggested volumetric flow rate, may explain the significant increase in generated force.

4.4 Critical Material Removal Rate and Burn Tests

The preceding tests have demonstrated the ability of the developed conditioner to generate a coherent jet, and to effectively deliver coolant to the grinding contact patch. However, the ultimate purpose of coolant delivery is to improve grinding performance [8]. The grinding burn test was carried out to determine the effectiveness of the coolant delivery on the grinding productivity, and the maximum depth of cut achievable before the onset of thermal damage.

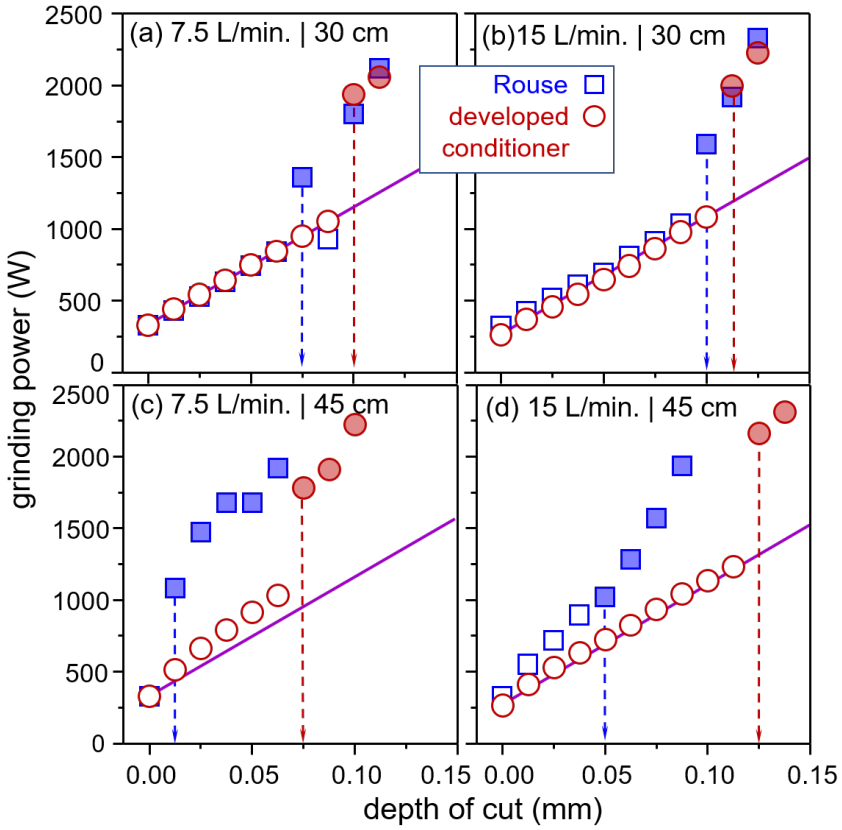

Figure 4.14: Grinding power measurements with noted burn

The results are plotted in figure 4.14, where open symbols represent non-burning cases, and filled in symbols denote burn. The onset of burn is also noted with vertical

dashed lines, showing the depth of cut. A linear trend was observed of the spindle power increasing with depth of cut, and before burn occurred the power increased 8.1 watts per micron of material removed. In each case, burn was clearly observed when the slope of the measured power increased beyond that trend. When divided by the feed rate and the workpiece width, the specific grinding energy prior to burn is determined to be 101 J/mm^3. This is in line with previously reported values as Marinescu et al, who state "[that i]n fine abrasive machining processes [...] the specific energy may be higher than 100 J/mm^3" [25].

In every case, the developed conditioner reached a greater depth of cut prior to grinding burn. The differences vary considerably between the different setups but, as detailed in table 4.2, range from a delta of 12.7 µm in the 15 L/min - 30 cm case to 63.5 µm in the two 45 cm cases. The benefits of a coherent jet which can more effectively deliver coolant, resulting in increased productivity, are clear.

Table 4.2: Maximum depths of cut before grinding burn

Jet Flow Rate	Stand-off Distance	Maximum Cutting Depth	
		Rouse nozzle	Developed conditioner
7.5 L/min	30 cm	63.5 µm	88.9 µm
	45 cm	0 µm	63.5 µm
15 L/min	30 cm	88.9 µm	101.6 µm
	45 cm	50.8 µm	114.3 µm

The impact of flow rate is clear to see as well. For each case of a consistent nozzle and stand off distance, the maximum depth of cut before burn increases significantly between the 15 and 30 m/s jet speeds.

Based on results from the dispersion, momentum flux, and particularly the hydrodynamic pressure experiments, expectations are that jet issuing from the developed conditioner at 30 m/s would be significantly more effective at delivering coolant to

the workpiece. The dispersion and momentum flux tests show that the developed conditioner generates a jet that maintains its shape at high velocities and stand-offs, which ensures that the coolant can be aimed effectively at the workpiece. The Rouse nozzle, by contrast, quickly diverges to over twice its initial diameter, which would necessitate that a large amount of fluid miss the grinding contact. Furthermore, the maximum delivered pressure in the momentum flux measurements does not show an obvious velocity core, which could have been masked by large surface waves in the optical investigations. The hydrodynamic pressure tests showed that the developed conditioner produced a force in the 15 L/min case more than 4 times greater than in the 7.5 L/min case, and in both cases outperformed the Rouse nozzle.

Based on these results, it is expected that a coherent jet traveling at 30 m/s would dramatically outperform all other jets, but that was not the case. The Rouse nozzle was able to adequately cool the workpiece in the majority of the cases, suggesting that though dispersed, adequate grinding fluid was delivered. While the developed conditioner outperformed the Rouse nozzle, at the 30 cm stand off distance it was only by 1 and by $\frac{1}{2}$ thousandths of an inch in the 7.5 L/min and 15 L/min cases, respectively. The difference is considerably more stark in the 45 cm stand off cases, but not to the point that earlier tests would suggest.

An intriguing result can be seen in figure 4.14a, after the onset of burn for the Rouse nozzle occurs at a cutting depth of 76.2 µm. Increasing the depth of cut further decreases the spindle power to below the non-burning trend line, after which it begins increasing again in line with the increase at the first burn point. This decrease in spindle power is suspected to be due to grinding wheel collapse, where rapid wheel wear changes the shape of the wheel, and leads to irregularities in the

grinding process [88].

Based on these tests, it is clear that the developed conditioner dramatically outperforms the Rouse nozzle in coolant delivery, increasing productivity and decreasing coolant waste. This is directly attributable to the generated coherent jet, and its precision and stability.

Chapter 5

Conclusion

A novel and highly effective flow conditioner and nozzle were developed, inspired by laminar fountains and wind tunnels. By conditioning the flow into a uniform laminar regime, through the use of uniform resistances and a honeycomb assembly, a simple cylindrical nozzle was found to generate a coherent jet, through the use of hydraulic flip. The system was characterized and compared to commercially available nozzles that purport to generate coherent cooling jets. The developed jet was found to display extreme coherence, appearing optically transparent and uniformly cylindrical at reasonable (<60 cm) stand off distances, to the point where text can be read through its surface. The jet diverged at a rate far less than the commercial jet, and remained within the conditions for coherence set in literature. The developed jet, with its known diameter and velocity, was used to investigate the air layer that surrounds a grinding wheel. A model predicting the critical velocity required to penetrate the air layer was developed, and validated with the developed jet. It was found that, contrary to conventional knowledge, the wheel surface can be wetted by a jet traveling at speeds that are an order of magnitude lower than the surface speed of

the wheel. The relative effective delivery rate was investigated, and a grinding burn experiment was conducted, to determine the real world effect of the coherent jet on coolant delivery and manufacturing productivity. The developed jet outperformed the commercial jet in all cases, if not to the extent expected.

The present work has contributed greatly to the state of the art, but further work remains. The developed conditioner has not been optimized for real world space or pumping pressure constraints, nor have the potential of the experiments begun here been fulfilled. The following areas are suggested for future work in the field of coherent jets and coolant delivery in grinding:

- Optimizing the design of the developed conditioner for space, pressure drop, and ease of mounting and positioning
- Investigate the free carrying capacity of the wheel surface.
- Determine the impact of flow conditioning on hydraulic flip, and opportunities for jet development.
- Adapt the simple aperture nozzle for more complicated uses, such as planar, elliptical, and profiled jets.
- Validate the developed model against a large range of wheel speeds.
- Apply the developed conditioner and coherent jet to grinding processes beyond surface grinding, such as gear and drill grinding
- Utilize the coherent jet in manufacturing applications other than grinding, such as turning or milling, to determine the impact of focused high speed cooling on the flank face of a tool.

Bibliography

[1] A. C. Shoemaker, M. I. Davies, and H. L. Moore, "Back to the Grindstone? The Archaeological Potential of Grinding-Stone Studies in Africa with Reference to Contemporary Grinding Practices in Marakwet, Northwest Kenya," *African Archaeological Review*, vol. 34, no. 3, pp. 415–435, Sep. 2017. [Online]. Available: http://link.springer.com/10.1007/s10437-017-9264-0

[2] J. C. Aurich, C. Effgen, and B. Kirsch, "Grinding," in *CIRP Encyclopedia of Production Engineering*, S. Chatti, L. Laperrière, G. Reinhart, and T. Tolio, Eds. Berlin, Heidelberg: Springer Berlin Heidelberg, 2019, pp. 795–799. [Online]. Available: https://doi.org/10.1007/978-3-662-53120-4_6427

[3] K. Wegener and C. Baumgart, "Grinding Burn," in *CIRP Encyclopedia of Production Engineering*, S. Chatti, L. Laperrière, G. Reinhart, and T. Tolio, Eds. Berlin, Heidelberg: Springer Berlin Heidelberg, 2019, pp. 800–806. [Online]. Available: https://doi.org/10.1007/978-3-662-53120-4_16786

[4] S. Malkin, "Grinding of metals: Theory and application," *Journal of Applied Metalworking*, vol. 3, no. 2, pp. 95–109, Jan. 1984. [Online]. Available: http://link.springer.com/10.1007/BF02833688

[5] M. Hacksteiner, H. Peherstorfer, and F. Bleicher, "Energy efficiency of state-of-the-art grinding processes," *Procedia Manufacturing*, vol. 21, pp. 717–724, 2018. [Online]. Available: https://linkinghub.elsevier.com/retrieve/pii/S2351978918302166

[6] J. Badger and A. Torrance, "Burn Awareness," *Cutting Tool Engineering*, vol. 52, no. 12, pp. 16–19, Dec. 2000. [Online]. Available: https://www.ctemag.com/sites/www.ctemag.com/files/archive_pdf/0012-burnawareness.pdf

[7] I. D. Marinescu, Ed., *Handbook of machining with grinding wheels*, ser. Manufacturing engineering and materials processing. Boca Raton, Fla: CRC / Taylor & Francis Group, 2007, no. 72.

[8] C. Heinzel, B. Kirsch, D. Meyer, and J. Webster, "Interactions of grinding tool and supplied fluid," *CIRP Annals*, vol. 69, no. 2, pp. 624–645, 2020. [Online]. Available: https://linkinghub.elsevier.com/retrieve/pii/S0007850620301347

[9] E. Brinksmeier, "Grinding Fluids," in *CIRP Encyclopedia of Production Engineering*, S. Chatti, L. Laperrière, G. Reinhart, and T. Tolio, Eds. Berlin, Heidelberg: Springer Berlin Heidelberg, 2019, pp. 806–809. [Online]. Available: https://doi.org/10.1007/978-3-662-53120-4_6428

[10] F. Engineer, C. Guo, and S. Malkin, "Experimental Measurement of Fluid Flow Through the Grinding Zone," *Journal of Manufacturing Science and Engineering*, vol. 114, no. 1, p. 61, Feb. 1992. [Online]. Available: http://manufacturingscience.asmedigitalcollection.asme.org/article.aspx?doi=10.1115/1.2899759

[11] S. Alenius and J. Johansson, "Air Flows and Particle Distribution Around a Rotating Grinding Wheel," *Aerosol Science and Technology*, vol. 25, no. 2, pp. 121–133, Jan. 1996. [Online]. Available: http://www.tandfonline.com/doi/abs/10.1080/02786829608965385

[12] V. Radhakrishnan and J. Rahman, "A Preliminary Investigation on the Condition of the Grinding Wheel Surface by Air Flow Measurements," *Annals of the CIRP*, vol. 25, no. 1, pp. 147–150, 1977.

[13] J. A. Webster, E. Brinksmeier, C. Heinzel, M. Wittmann, and K. Thoens, "Assessment of Grinding Fluid Effectiveness in Continuous-Dress Creep Feed Grinding," *CIRP Annals*, vol. 51, no. 1, pp. 235–240, 2002. [Online]. Available: https://linkinghub.elsevier.com/retrieve/pii/S0007850607615078

[14] T. Akiyama, J. Shibata, and S. Yonetsu, "Behavior of grinding fluid in the gap of the contact area between a grinding wheel and a workpiece," 1984, pp. 55–57.

[15] S. Ebbrell, N. Woolley, Y. Tridimas, D. Allanson, and W. Rowe, "The effects of cutting fluid application methods on the grinding process," *International Journal of Machine Tools and Manufacture*, vol. 40, no. 2, pp. 209–223, Jan. 2000. [Online]. Available: http://linkinghub.elsevier.com/retrieve/pii/S0890695599000607

[16] I. Inasaki, "Fluid Films in the Grinding Arc of Contact," Paris, France, Jan. 1998, courtesy of the CIRP Archives.

[17] B. Mandal, S. Majumdar, S. Das, and S. Banerjee, "Formation of a significantly less stiff air-layer around a grinding wheel pasted with rexine leather,"

International Journal of Precision Technology, vol. 2, no. 1, p. 12, 2011. [Online]. Available: http://www.inderscience.com/link.php?id=38106

[18] G. Trmal and H. Kaliszer, "Delivery of Cutting Fluid in Grinding," *Chartered Mechanical Engineering*, vol. 23, no. 8, pp. 95–100, Sep. 1976.

[19] A. Lopez-Arraiza, G. Castillo, H. N. Dhakal, and R. Alberdi, "High performance composite nozzle for the improvement of cooling in grinding machine tools," *Composites Part B: Engineering*, vol. 54, pp. 313–318, Nov. 2013. [Online]. Available: http://linkinghub.elsevier.com/retrieve/pii/S1359836813002837

[20] J. Webster, C. Cui, R. Mindek, and R. Lindsay, "Grinding Fluid Application System Design," *CIRP Annals*, vol. 44, no. 1, pp. 333–338, 1995. [Online]. Available: http://linkinghub.elsevier.com/retrieve/pii/S0007850607623373

[21] A. Hosokawa, K. Tokunaga, T. Ueda, T. Kiwata, and T. Koyano, "Drastic reduction of grinding fluid flow in cylindrical plunge grinding by means of contact-type flexible brush-nozzle," *CIRP Annals*, vol. 65, no. 1, pp. 317–320, 2016. [Online]. Available: http://linkinghub.elsevier.com/retrieve/pii/S0007850616300920

[22] C.-C. Chang, "An analysis of coolant flow and heat transfer in grinding," Ph.D. dissertation, University of Pittsburgh, 1994.

[23] E. Brinksmeier, A. Walter, R. Janssen, and P. Diersen, "Aspects of cooling lubrication reduction in machining advanced materials," *Proceedings of the Institution of Mechanical Engineers, Part B: Journal of Engineering*

Manufacture, vol. 213, no. 8, pp. 769–778, Aug. 1999. [Online]. Available: http://journals.sagepub.com/doi/10.1243/0954405991517209

[24] N. Madanchi, M. Winter, S. Thiede, and C. Herrmann, "Energy Efficient Cutting Fluid Supply: The Impact of Nozzle Design," *Procedia CIRP*, vol. 61, pp. 564–569, 2017. [Online]. Available: http://linkinghub.elsevier.com/retrieve/pii/S221282711631352X

[25] I. D. Marinescu, W. Brian Rowe, Boris Dimitrov, and Ichiro Inasaki, *Tribology of abrasive machining processes*. Norwich, NY: William Andrew Pub, 2004.

[26] C. Guo and S. Malkin, "Energy Partition and Cooling During Grinding," *Journal of Manufacturing Processes*, vol. 2, no. 3, pp. 151–157, Jan. 2000. [Online]. Available: https://linkinghub.elsevier.com/retrieve/pii/S1526612500701162

[27] M. C. Shaw, "Some Observations Concerning the Mechanics of Cutting and Grinding," *Applied Mechanics Reviews*, vol. 46, no. 3, pp. 74–79, Mar. 1993. [Online]. Available: https://asmedigitalcollection.asme.org/appliedmechanicsreviews/article/46/3/74/421526/Some-Observations-Concerning-the-Mechanics-of

[28] J. A. Webster, "Coolant calculus," *Cutting Tool Engineering*, vol. 60, no. 2, pp. 58–66, Feb. 2008. [Online]. Available: https://www.ctemag.com/news/articles/coolant-calculus

[29] ——, "In grinding coolant application matters," *Manufacturing engineering*, vol. 140, no. 3, pp. 171–+, 2008.

[30] P. De Aguiar, F. Dotto, and E. Bianchi, "Study of thresholds to burning in surface grinding process," *Journal of the Brazilian Society of Mechanical Sciences and Engineering*, vol. 27, no. 2, pp. 150–156, Jun. 2005. [Online]. Available: http://www.scielo.br/scielo.php?script=sci_arttext&pid=S1678-58782005000200007&lng=en&nrm=iso&tlng=en

[31] A. Faghri and Y. Zhang, *Fundamentals of Multiphase Heat Transfer and Flow*. Cham: Springer International Publishing, 2020. [Online]. Available: http://link.springer.com/10.1007/978-3-030-22137-9

[32] A. Jackson, "An investigation of useful fluid flow in grinding," PhD, Liverpool John Moores University, Liverpool, UK, 2008. [Online]. Available: http://researchonline.ljmu.ac.uk/id/eprint/5860

[33] W. B. Rowe, *Principles of modern grinding technology*, 2nd ed. William Andrew, 2014.

[34] M. N. Morgan, A. Jackson, H. Wu, V. Baines-Jones, A. Batako, and W. Rowe, "Optimisation of fluid application in grinding," *CIRP Annals*, vol. 57, no. 1, pp. 363–366, 2008. [Online]. Available: http://linkinghub.elsevier.com/retrieve/pii/S0007850608000772

[35] S. Malkin and C. Guo, "Vitrified Wheel Composition and Phase Diagrams," in *Grinding technology theory and application of machining with abrasives*, 2nd ed., 2008.

[36] S. Mihić, R. Dražumerič, F. Pušavec, J. Badger, and P. Krajnik, "The use of computational fluid dynamics in the analysis of fluid flow and thermal aspects in

grinding," *Proceedings of the Institution of Mechanical Engineers, Part B: Journal of Engineering Manufacture*, vol. 231, no. 12, pp. 2103–2111, Oct. 2017. [Online]. Available: http://journals.sagepub.com/doi/10.1177/0954405415624657

[37] V. Gviniashvili, J. Webster, and B. Rowe, "Fluid Flow and Pressure in the Grinding Wheel-Workpiece Interface," *Journal of Manufacturing Science and Engineering*, vol. 127, no. 1, p. 198, 2005. [Online]. Available: http://ManufacturingScience.asmedigitalcollection.asme.org/article.aspx?articleid=1449556

[38] H. Sakamoto, K. Kajiwara, S. Shimizu, and S. Ohmori, "Mechanism of Improvement Effect of Ultrasonically Activated Coolant on Finished Surface Roughness in Cylindrical Grinding," *JSME International Journal Series C*, vol. 49, no. 2, pp. 346–352, 2006. [Online]. Available: http://joi.jlc.jst.go.jp/JST.JSTAGE/jsmec/49.346?from=CrossRef

[39] S. Majumdar, S. Kumar, D. Roy, and S. Chakraborty, "Improvement of Lubrication and Cooling in Grinding by Effective Controlling of Air Boundary," *International Journal of Industrial and Manufacturing Systems Engineering*, vol. 2, no. 6, p. 72, 2018.

[40] B. Kirsch, "The impact of contact zone flow rate and bulk cooling on the cooling efficiency in grinding applying different nozzle designs and grinding wheel textures," *CIRP Journal of Manufacturing Science and Technology*, vol. 18, pp. 179–187, Aug. 2017. [Online]. Available: http://linkinghub.elsevier.com/retrieve/pii/S1755581717300056

[41] B. Mandal, D. Biswas, A. Sarkar, S. Das, and S. Banerjee, "Grinding Performance Using a Compound Nozzle Characterised by Small Discharge of Fluid," *Journal of the Association of Engineers, India*, vol. 83, no. 1, p. 28, Mar. 2013. [Online]. Available: http://www.i-scholar.in/index.php/JAEI/article/view/119916

[42] C. Heinzel, D. Meyer, B. Kolkwitz, and J. Eckebrecht, "Advanced approach for a demand-oriented fluid supply in grinding," *CIRP Annals*, vol. 64, no. 1, pp. 333–336, 2015. [Online]. Available: http://linkinghub.elsevier.com/retrieve/pii/S0007850615000177

[43] D. Liu, G. Wang, Z. Nie, and Y. K. Rong, "An in-situ infrared temperature-measurement method with back focusing on surface for creep-feed grinding," *Measurement*, vol. 94, pp. 645–652, Dec. 2016. [Online]. Available: http://www.sciencedirect.com/science/article/pii/S0263224116305139

[44] C. Li, Q. Zhang, S. Wang, D. Jia, D. Zhang, Y. Zhang, and X. Zhang, "Useful fluid flow and flow rate in grinding: an experimental verification," *The International Journal of Advanced Manufacturing Technology*, vol. 81, no. 5-8, pp. 785–794, Nov. 2015. [Online]. Available: http://link.springer.com/10.1007/s00170-015-7230-z

[45] J. Steffen, "Application of a coherent jet coolant system in creep-feed grinding of Inconel 718." Master's thesis, Dalhousie, Halifax, Nova Scotia, 2005.

[46] The International Academy for Production Engineering, *CIRP Encyclopedia of Production Engineering*, S. Chatti, L. Laperrière, G. Reinhart, and T. Tolio,

Eds. Berlin, Heidelberg: Springer Berlin Heidelberg, 2019. [Online]. Available: http://link.springer.com/10.1007/978-3-662-53120-4

[47] E. Brinksmeier, C. Heinzel, and M. Wittmann, "Friction, Cooling and Lubrication in Grinding," *CIRP Annals*, vol. 48, no. 2, pp. 581–598, 1999. [Online]. Available: http://linkinghub.elsevier.com/retrieve/pii/S0007850607632363

[48] Advanced Manufacturing Technology Research Institute, "High-Speed grinding with particular reference to the proper employment of grinding fluids," AMTRI, Macclesfield, Tech. Rep., 1973.

[49] C. Baumgart, J. J. Radziwill, F. Kuster, and K. Wegener, "A Study of the Interaction between Coolant Jet Nozzle Flow and the Airflow Around a Grinding Wheel in Cylindrical Grinding," *Procedia CIRP*, vol. 58, pp. 517–522, 2017. [Online]. Available: http://linkinghub.elsevier.com/retrieve/pii/S2212827117304444

[50] T. Davies and R. Jackson, "Air flow around grinding wheels," *Precision Engineering*, vol. 3, no. 4, pp. 225–228, Oct. 1981. [Online]. Available: http://linkinghub.elsevier.com/retrieve/pii/0141635981900970

[51] B. Mandal, R. Singh, S. Das, and S. Banerjee, "Development of a Grinding Fluid Delivery Technique and Its Performance Evaluation," *Materials and Manufacturing Processes*, vol. 27, no. 4, pp. 436–442, Apr. 2012. [Online]. Available: http://www.tandfonline.com/doi/abs/10.1080/10426914.2011.585487

[52] B. Qiu, J. Yin, W. Ding, J. Xu, and Q. Guo, "Flow field and cooling capacity in workpiece-tool contact zone during ultra-high speed grinding," *The International Journal of Advanced Manufacturing Technology*, vol. 111, no. 7-8, pp. 2349–2359, Dec. 2020. [Online]. Available: http://link.springer.com/10.1007/s00170-020-06295-6

[53] C. Cui, "Experimental investigation of thermo-fluid effects in the grinding zone." PhD, University of Connecticut, 1996. [Online]. Available: https://opencommons.uconn.edu/dissertations/AAI9538308/

[54] V. Gviniashvili, N. Woolley, and W. Rowe, "Useful coolant flowrate in grinding," *International Journal of Machine Tools and Manufacture*, vol. 44, no. 6, pp. 629–636, May 2004. [Online]. Available: http://linkinghub.elsevier.com/retrieve/pii/S0890695503003134

[55] C. Li, G. Y. Liu, Y. L. Hou, Y. C. Ding, and B. H. Lu, "Modeling and experimental investigation of useful flow-rate in flood delivery grinding." IEEE, Jun. 2009, pp. 5467–5471. [Online]. Available: http://ieeexplore.ieee.org/document/5191857/

[56] G. K. Batchelor, *An Introduction to Fluid Dynamics*, 1st ed. Cambridge University Press, Feb. 2000. [Online]. Available: https://www.cambridge.org/core/product/identifier/9780511800955/type/book

[57] R. P. Grant and S. Middleman, "Newtonian jet stability," *AIChE Journal*, vol. 12, no. 4, pp. 669–678, Jul. 1966. [Online]. Available: http://doi.wiley.com/10.1002/aic.690120411

[58] V. A. Baines-Jones, M. Morgan, A. Batako, E. Brown, and G. AMTReL, "Modelling and simulation of grinding fluid nozzles," in *Advances in Manufacturing Technology–XXII*, Brunel University, UK, Sep. 2008, p. 631.

[59] V. A. Baines-Jones, "Nozzle design for improved useful fluid flow in grinding," PhD, Liverpool John Moores University, Liverpool, UK, 2010. [Online]. Available: http://ethos.bl.uk/OrderDetails.do?uin=uk.bl.ethos.515347

[60] M. N. Morgan and V. Baines-Jones, "On the Coherent Length of Fluid Nozzles in Grinding," *Key Engineering Materials*, vol. 404, pp. 61–67, 2009. [Online]. Available: https://www.scientific.net/KEM.404.61

[61] P. Geilert, C. Heinzel, and A. Wagner, "Grinding Fluid Jet Characteristics and Their Effect on a Gear Profile Grinding Process," *Inventions*, vol. 2, no. 4, p. 27, Oct. 2017. [Online]. Available: http://www.mdpi.com/2411-5134/2/4/27

[62] A. Warkentin, R. Bauer, and D. Hartlen, "Comparison of conventional, coherent-jet and high-pressure coolant delivery systems for profile grinding," *Transactions of the Canadian Society for Mechanical Engineering*, vol. 32, no. 1, pp. 107–120, 2008.

[63] B. St-Pierre, J.-F. Chatelain, and L. Dufresne, "Developpement d'un Modele Semi-Empirique pour la Prediction de la Coherence d'un Jet Utilise Dans les Procedes de Rectification," *Transactions of the Canadian Society for Mechanical Engineering*, vol. 36, no. 2, pp. 127–142, 2012. [Online]. Available: http://www.nrcresearchpress.com/doi/10.1139/tcsme-2012-0009

[64] R. A. Irani, R. J. Bauer, and A. Warkentin, "Development of a new cutting fluid delivery system for creepfeed grinding," *International Journal of Manufacturing Technology and Management*, vol. 12, no. 1/2/3, p. 108, 2007. [Online]. Available: http://www.inderscience.com/link.php?id=14157

[65] E. Rouly, A. Warkentin, and R. Bauer, "Design and testing of low-divergence elliptical-jet nozzles," *Journal of Mechanical Science and Technology*, vol. 29, no. 5, pp. 1993–2003, May 2015. [Online]. Available: http://link.springer.com/10.1007/s12206-015-0420-7

[66] J. W. Hoyt, J. J. Taylor, and C. D. Runge, "The structure of jets of water and polymer solution in air," *Journal of Fluid Mechanics*, vol. 63, no. 4, pp. 635–640, May 1974. [Online]. Available: https://www.cambridge.org/core/article/structure-of-jets-of-water-and-polymer-solution-in-air/6C2FCFF6AE7AF611A43DF1FF9C425E07

[67] T. Nguyen, D. Shanmugam, and J. Wang, "Effect of liquid properties on the stability of an abrasive waterjet," *International Journal of Machine Tools and Manufacture*, vol. 48, no. 10, pp. 1138–1147, Aug. 2008. [Online]. Available: http://linkinghub.elsevier.com/retrieve/pii/S0890695508000278

[68] H. Rouse, "Experimental investigation of fire monitors and nozzles," vol. 77. ASCE, 1951, pp. 1–29.

[69] M. McCarthy and N. Molloy, "Review of stability of liquid jets and the influence of nozzle design," *The Chemical Engineering Journal*, vol. 7, no. 1, pp. 1–20, Jan. 1974. [Online]. Available: http://linkinghub.elsevier.com/retrieve/pii/0300946774800213

[70] J. W. Hoyt and J. J. Taylor, "Effect of Nozzle Shape and Polymer Additives on Water Jet Appearance," *Journal of Fluids Engineering*, vol. 101, no. 3, pp. 304–308, Sep. 1979. [Online]. Available: https://asmedigitalcollection.asme.org/fluidsengineering/article/101/3/304/439551/Effect-of-Nozzle-Shape-and-Polymer-Additives-on

[71] R. A. Irani, R. Bauer, and A. Warkentin, "A review of cutting fluid application in the grinding process," *International Journal of Machine Tools and Manufacture*, vol. 45, no. 15, pp. 1696–1705, Dec. 2005. [Online]. Available: http://linkinghub.elsevier.com/retrieve/pii/S0890695505000751

[72] R. L. Stoker, "Methods of Producing Uniform Velocity Distribution." *Industrial & Engineering Chemistry*, vol. 38, no. 6, pp. 622–624, Jun. 1946. [Online]. Available: https://pubs.acs.org/doi/abs/10.1021/ie50438a024

[73] C. Farell and S. Youssef, "Experiments on Turbulence Management Using Screens and Honeycombs," *Journal of Fluids Engineering*, vol. 118, no. 1, pp. 26–32, Mar. 1996. [Online]. Available: http://dx.doi.org/10.1115/1.2817505

[74] Y. A. Çengel and J. M. Cimbala, *Fluid mechanics: fundamentals and applications*, fourth edition ed. New York, NY: McGraw-Hill Education, 2018.

[75] R. I. Loehrke and H. M. Nagib, "Control of Free-Stream Turbulence by Means of Honeycombs: A Balance Between Suppression and Generation," *Journal of Fluids Engineering*, vol. 98, no. 3, pp. 342–351, Sep. 1976. [Online]. Available: https://asmedigitalcollection.asme.org/fluidsengineering/article/98/3/342/442092/Control-of-FreeStream-Turbulence-by-Means-of

[76] H. Chaves, M. Knapp, A. Kubitzek, F. Obermeier, and T. Schneider, "Experimental Study of Cavitation in the Nozzle Hole of Diesel Injectors Using Transparent Nozzles," Feb. 1995. [Online]. Available: https://www.sae.org/content/950290/

[77] J. Iciek, "The hydrodynamics of a free, liquid jet and their influence on direct contact heat transfer—II Conditions of change of liquid outflow type through sharp inlet edged orifice," *International Journal of Multiphase Flow*, vol. 8, no. 3, pp. 251–260, Jun. 1982. [Online]. Available: http://www.sciencedirect.com/science/article/pii/0301932282900349

[78] D. Moyo, "Characterisation and Optimisation of Waterjet Impact Forces and Energy Parameters During Hydroentanglement," PhD, Nelson Mandela Metropolitan University, 2012. [Online]. Available: http://hdl.handle.net/10948/d1020134

[79] T. J. Chew, "Hydraulic Flip Behavior in Typical Liquid Rocket Operating Regimes," Edwards Air Force Base, Air Force Rocket Propulsion Lab, Technical Reports AD-764 730, Jul. 1973. [Online]. Available: https://apps.dtic.mil/dtic/tr/fulltext/u2/764730.pdf

[80] A. Sou, S. Hosokawa, and A. Tomiyama, "Effects of cavitation in a nozzle on liquid jet atomization," *International Journal of Heat and Mass Transfer*, vol. 50, no. 17-18, pp. 3575–3582, Aug. 2007. [Online]. Available: https://linkinghub.elsevier.com/retrieve/pii/S0017931007001019

[81] R. P. Benedict, N. A. Carlucci, and S. D. Swetz, "Flow Losses in Abrupt Enlargements and Contractions," *Journal of Engineering for Gas Turbines*

and Power, vol. 88, no. 1, pp. 73–81, Jan. 1966. [Online]. Available: https://doi.org/10.1115/1.3678482

[82] J. H. Lienhard and J. H. Lienhard, "Velocity Coefficients For Free Jets From Sharp-Edged Orifices," *Journal of Fluids Engineering*, vol. 106, no. 1, pp. 13–17, Mar. 1984. [Online]. Available: https://asmedigitalcollection.asme.org/fluidsengineering/article/106/1/13/406906/Velocity-Coefficients-For-Free-Jets-From

[83] J. H. Bell and R. D. Mehta, "Contraction design for small low-speed wind tunnels," Joint Institute for Aeronautics and Acoustics, Ames Research Center, Tech. Rep. JIAA TR-84, Apr. 1988. [Online]. Available: https://purl.fdlp.gov/GPO/LPS112064

[84] D. Feng, L. Shi, C. Guo, F. Wang, and Y. Chen, "Numerical and experimental study on the flow characteristics of abrasive slurry jet with polymer additives," *The International Journal of Advanced Manufacturing Technology*, vol. 95, no. 9-12, pp. 3289–3299, Apr. 2018. [Online]. Available: http://link.springer.com/10.1007/s00170-017-1371-1

[85] E. v. Wijk, "Micro-machining with Abrasive Slurry-Jets: Effects of Dissolved Polymer Concentration and Nozzle Design," *The International Journal of Advanced Manufacturing Technology*, no. 102, pp. 317–331, Jan. 2019.

[86] G. I. Taylor, G. K. Batchelor, H. L. Dryden, and G. B. Schubauer, "The effect of wire gauze on small disturbances in a uniform stream," *The Quarterly Journal of Mechanics and Applied Mathematics*, vol. 2, no. 1, pp. 1–29, Jan. 1949. [Online]. Available: https://academic.oup.com/qjmam/article/2/1/1/1889399

[87] M. Ganesan, C Guo, A Ronen, and S Malkin, "Analysis of Hydrodynamic Forces in Grinding," vol. 24. Dearborn, Mich: Society of Manufacturing Engineers, 1996, pp. 105–110.

[88] J. Badger, "Factors affecting wheel collapse in grinding," *CIRP Annals*, vol. 58, no. 1, pp. 307–310, 2009. [Online]. Available: https://linkinghub.elsevier.com/retrieve/pii/S0007850609000936